Comprehensive analysis of a novel integration of a biomass-driven combined heat and power plant with a compressed air energy storage (CAES)

Lashgari, Fatemeh; Babaei, Seyed Mostafa; Pedram, Mona Zamani; Arabkoohsar, Ahmad

Published in:
Energy Conversion and Management

DOI (link to publication from Publisher):
10.1016/j.enconman.2022.115333

Publication date:
2022

Document Version
Publisher's PDF, also known as Version of record

Energy Conversion and Management 255 (2022) 115333

Contents lists available at ScienceDirect

Energy Conversion and Management

journal homepage: www.elsevier.com/locate/enconman

Comprehensive analysis of a novel integration of a biomass-driven combined heat and power plant with a compressed air energy storage (CAES)

Fatemeh Lashgari [a], Seyed Mostafa Babaei [a], Mona Zamani Pedram [a,*], Ahmad Arabkoohsar [b,*]

[a] Department of Mechanical Engineering, K.N. Toosi University of Technology, Tehran, Iran
[b] Energy Department, Aalborg University, Denmark

ARTICLE INFO

Keywords:
Biomass gasification
CAES
CHP
Flue gas condensation
Thermoeconomic

ABSTRACT

Unlike wind and solar energy, biomass is capable of providing stable and controllable energy output in an energy system at zero or even negative net emission rate. The combination of a gasification unit with a Brayton cycle is one of the traditional methods of utilizing biomass resources. This work presents a thorough (Energy, Exergy, Economic, Exergoeconomic, and Environmental) analysis of a biomass-driven combined heat and power (CHP), via a gasifier, with a compressed air energy storage (CAES) unit. The hybrid system is capable of multi-generating heat and power as well as contributing to load shifting and peak shaving for the electricity grid. With about 71% and 47% of total and electrical round-trip efficiencies, the proposed system demonstrates 67% and 12% efficiency improvement in comparison to the stand-alone biomass power plant. 348.4 MWh is the net produced power each day and 50% of this amount is generated during the on-peak period. Also, 6651.4 m^3 domestic hot water is produced during the 24-hour operation of the system. The Levelized Cost of Electricity (LCOE) of the system is around 0.05 $/kWh with an average electricity price of 0.1 $/kWh elaborating the economic potentials of the system. The payback period and total profit of around 2 years and 181 M$ further prove the economic feasibility of the proposed system. Moreover, due to obtained results from the environmental analysis, it is proved that the introduced system is capable of capturing 25,764 tonnes/year CO_2 emission from the atmosphere.

1. Introduction

Over 80% of the world's energy is still supplied by fossil fuels, which are responsible for severe environmental problems such as air pollution, global warming, ocean acidification, etc. [1]. Numerous protocols have been ratified to eliminate the potential damages caused by fossil fuels, one of the most vital of which is harvesting energy from green and renewable sources [2]. That is why the endeavors in the path of energy generation from green sources and sustainable methods have increased dramatically over the recent years. The recent techno-economic advances in the technologies harvesting wind and solar energy have made them two of the most important renewable options for green energy supply but they still suffer from their main drawback which is a fluctuating nature, leading to stochastic energy output, and dependence on weather conditions [3]. This can be addressed by other renewable sources which do not suffer from the same weakness and energy storage technologies [4].

With the possibility of net negative carbon emissions, great availability, and lower costs, biomass is an interesting option for a green yet stable energy supply, independent of the weather conditions and environmental restrictions. Biomass can be directly used as a fuel or be converted to other products so-called biofuels [5]. There are two common methods (biochemical and thermochemical) for the conversion of biomass into fuel and chemical products. In thermochemical conversion, the major processes are direct combustion, pyrolysis, and gasification. Char gasification is a well-known method extensively used to produce syngas out of carbonaceous solids with a high volumetric capacity and low emission rate. For a standard gasification process drying, thermal decomposition (pyrolysis), combustion, and eventually gasification is taking place in an oxygen-starved condition in specified temperature ranges [5,6]. A power plant based on the gasification process is

* Corresponding authors.
E-mail addresses: fatemeh.lashgari129@gmail.com (F. Lashgari), s.mostafababaei@gmail.com (S.M. Babaei), m.zpedram@kntu.ac.ir (M.Z. Pedram), ahm@energy.aau.dk (A. Arabkoohsar).

https://doi.org/10.1016/j.enconman.2022.115333
Received 9 December 2021; Received in revised form 15 January 2022; Accepted 4 February 2022
Available online 15 February 2022

Nomenclature

A	Area [m^2]
c	Cost per exergy [$/GJ]
$\dot{C}$	Cost rate of exergy [$/hr]
$\dot{E}x$	Exergy rate [kW]
$\overline{ex}_{Ch}$	Molar chemical exergy [kJ/kmol]
f	Molar fraction
f_k	Exergoeconomic factor [%]
h	Enthalpy [kJ/kg]
$\overline{h}_f^0$	Enthalpy of formation [kJ/kmol]
i	Interest rate [%]
M	Molar mass [kg/mol]
$\dot{m}$	Mass flow rate [kg/s]
N	System lifespan [year]
P	Pressure [bar]
$\dot{Q}$	Heat transfer rate [kW]
R	Universal gas constant [J/mol·K]
r	Discount rate [%]
r_k	Relative cost difference [%]
s	Entropy [kJ/kg·K]
T	Temperature [K]
t	Time [hour]
V	Volume [m^3]
$\dot{W}$	Power [kW]
Y	Cash flow [M$]
Z	Cost function [$]
$\dot{Z}$	Cost rate [$/hr]
$\Delta\overline{h}$	Enthalpy difference [kJ/kmol]
η	Isentropic efficiency [%]
ϕ	Maintenance factor [%]
τ	Annual operating hours [hour]

Abbreviations

AC	Air compressor
Aftc	Aftercooler
ASED	Air storage energy density [MJ/m^3]
AT	Air turbine
BC	Brayton cycle
CAES	Compressed air energy storage
CC	Combustion chamber
CHP	Combined heat and power
Con	Condenser
COT	Cold oil tank
CRF	Capital recovery factor
DHW	Domestic hot water
ERTE	Exergetic round trip efficiency [%]
ESS	Energy storage system
Ev	Evaporator
Evp	Expansion valve
FA	Fuel-air ratio
FGC	Flue gas condensation
Ge	Generator
GHG	Greenhouse gas
HHV	Higher heating value [kJ/kg]
HOT	Hot oil tank
HWT	Hot water tank
Hx	Heat exchanger
Intc	Intercooler
LCA	Life Cycle Assessment
LCOE	Levelized cost of electricity [$/GJ]
LHV	Lower heating value [kJ/kg]
MC	Moisture content [%]
Mt	Motor
M&S	Marshall and Swift factor
NPV	Net present value [M$]
ORC	Organic rankine cycle
OT	ORC Turbine
P	Pump
PP	Payback period [year]
PtP	Pump-to-Product
RC	Rankine cycle
Rec	Recuperator
Reg valve	Regulation valve
RSE	Renewable sources of energy
RTE	Round trip efficiency [%]
ST	Steam turbine
SUCP	Sum unit cost of product [$/GJ]
TES	Thermal energy storage
WHR	Waste heat recovery
WtP	Well-to-Pump

Subscripts

0	Dead state
Ch	Chemical
ch	Charge
dch	Discharge
EnvSave	Environmental saving
in	Inlet
k	kth component
out	Outlet
s	Isentropic state
T	Turbine
tot	Total
W	Work

Superscripts

D	Destruction
f	Fuel
p	Product
W	Work

thermodynamically analyzed by Habibollahzade et al. [7]. They carried out the thermoeconomic assessment for the optimized version of the system. A medium-sized gasification plant had been analyzed by Wu et al. [8]. The main focus of this study was on the impact of moisture content and equivalence ratio. The combination of the biomass gasification process with other renewable energy types is another popular topic among the different investigations in this field. For instance, Khalid et al. [9] performed energy and exergy assessments on a multi-generating energy system based on biomass and solar energies. Based upon the obtained results, the proposed system performed better in the case of utilizing both sources of energy rather than the case which uses each one of the sources.

Multi-generation energy systems, e.g. CHP plants, are the unavoidably vital elements of energy systems in the future where there should be maximum utilization of energy availabilities and inter-sector couplings [10]. CHP plants could be very compatibly run directly by biomass sources or sub-products after pyrolysis or gasification [5]. Biomass-based CHP plants have gained a lot of attention in recent decades where about one-fifth of the total required energy in Finland is generated by bioresources [11]. In Austria and Sweden, the portion of

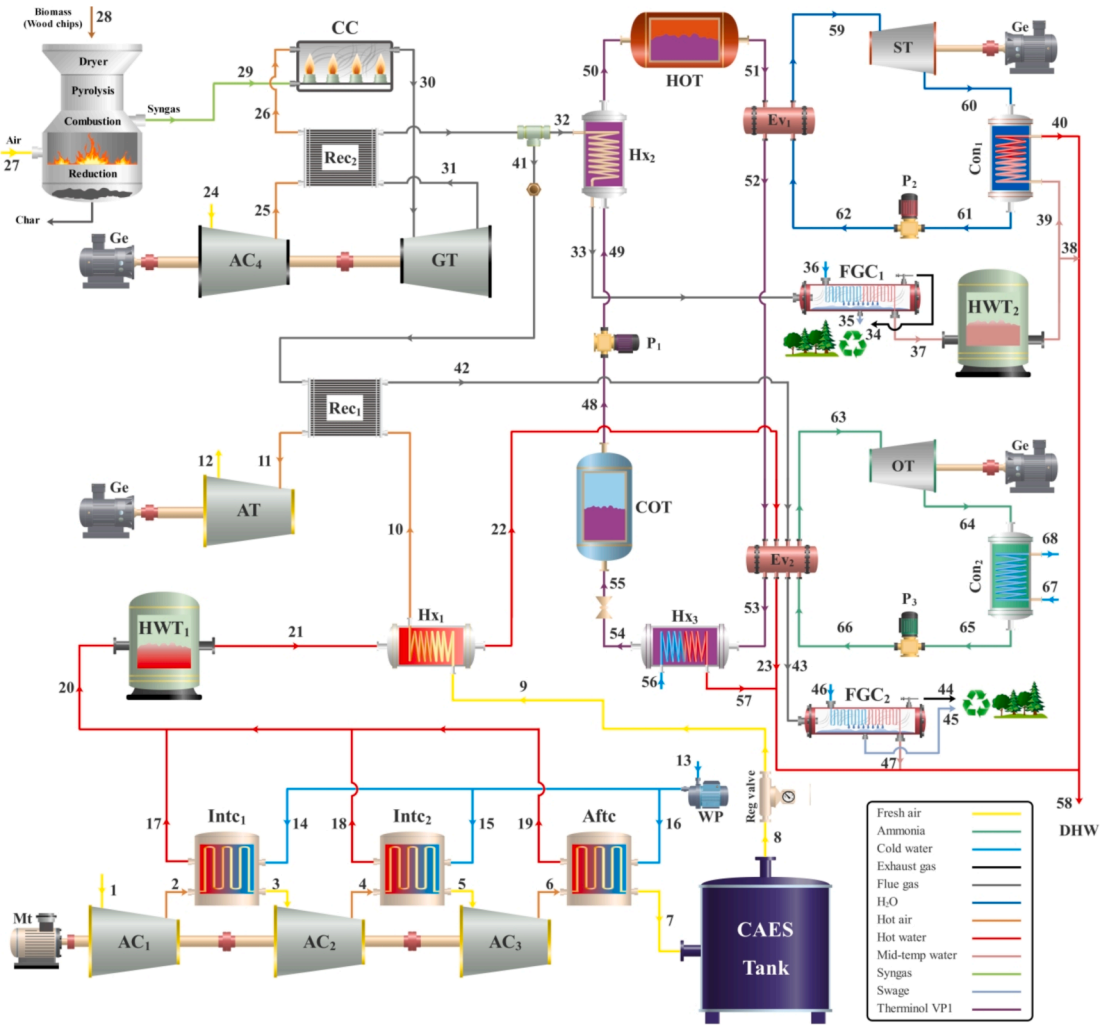

Fig. 1. The outline of the biomass-based CHP plant integrated with the CAES system.

bioresources for district heating purposes has seen six-fold and eight-fold increment in the last decade [12]. In the field of biomass-driven CHP plants, a lot of investigation had been done. The energetic and environmental performances of a CHP plant based on the gasification process are assessed by Gholamian et al. [13]. Wood and paper were utilized as the biomass feedstocks of this system. 40.1% and 39.1% were the efficiency of this system in case of using wood and paper fuels. Also, the CO_2 emission was higher for wood fuel rather than the paper feedstock. In another investigation, Ahmadi et al. [14] analyzed a multi-generating system thermodynamically. Finally, they concluded that multi-generation systems are more environmentally friendly than single-generating systems.

Compressed air energy storage (CAES) is one of the most important and reliable energy storage technologies for large capacities, which can also be integrated with any renewable power cycle. This will of course be of direct impact if the energy storage unit is coupled with a solar or wind energy plant but still of high value for scaling up the peak production capacity of any other type of plants, including biomass-driven CHP plants while acting as an asset for utilizing the off-peak cheap electricity of the grid which is dominated by solar and wind plants [10]. Also, in terms of running remote biomass-based power plants, energy storage systems like CAES can play important roles in the independent operation of these power plants by load leveling of energy production/consumption patterns. Electricity consumption profiles in residential and commercial segments show on-peak, mid-peak, and off-peak periods which should be organized and matched with the output of the production chain [15]. The produced electricity in off-peak times which is cheaper than other periods can be stored and then be released in specific hours called “peak times” [16]. Numerous investigators have studied and analyzed different aspects of CAES systems in both cases of stand-alone and integrated with different energy systems. Comparison of CAES integration with a wind farm and a natural gas combined-cycle was accomplished by Mason et al. [17]. They found these two hybridizations competitive in terms of economy but the CAES-Wind combination overtook the combined-cycle in terms of fuel consumption and consequently environmental issues. Razmi et al. [15] analyzed a novel integrated system consisting of a CAES unit and an absorption-recompression refrigeration system. The outputs of this investigation were 2287 kW cooling in a system with about 57% round-trip efficiency (RTE) and a payback period shorter than 6 years. The same team developed their innovative CAES configuration by combining different technologies like high-temperature energy storage [18] and multi-effect desalination units [19]. A combined cooling, heating, and power system based on an integrated solar-CAES system was assessed and optimized from a thermodynamic viewpoint by Wang et al. [20]. Hybridization of CAES with solid oxide fuel cell and turbocharger was investigated by Roushenas et al. [21].

In terms of providing flexibility to the biomass power plant, the integration of this system with a grid-scale energy storage unit like a CAES system as one of the most promising ones is a potential solution to address the mismatch between production and demand of the grid. The results of this article will later show how such a combination

outperforms stand-alone and old-fashioned concepts of biomass-based CHP plants. In fact, a multi-generating energy system comprising a biomass gasification plant with a CAES system and a cascade waste heat recovery (WHR) unit consisting of a Brayton cycle (BC), Rankine cycle (RC), and an Organic Rankine cycle (ORC) is proposed and investigated in this work. The proposed configuration is scrutinized from Energy, Exergy, Economic, Exergoeconomic and, Environmental perspectives. Thermal energy storage (TES) and flue gas condensation (FGC) units are employed in different parts of the system in order to gain the maximum possible efficiencies throughout the whole system processes. Besides being environmentally friendly by negative-carbon characteristics of biomass, the introduced system in this investigation showed a lot of superiorities to the other similar systems in the literature. In addition to the remarkable improvements in thermodynamic efficiencies, the proposed system demonstrated better economic performance than a basic biomass CHP plant. In the following sections, the proposed system is described in detail. Then the governing equations are expressed and the simulation method is validated using scientific and experimental results available in the literature. Eventually, thorough analyses results are presented and discussed to provide a deep comprehension of the system performance, strengths, weaknesses, further improvement opportunities, etc.

2. System description

The schematic of the proposed system in this study is illustrated in Fig. 1. This system consists of a stand-alone biomass power plant (gasification + BC) and a cascade WHR system including RC and ORC beside FGC and DHW production units. This configuration is coupled with a CAES system which further upgrades the stability of the system. The proposed system is capable of multi-generating heat and power with a more technical approach in the field of energy management. Peak shaving/shifting and load leveling are some other substantial features of the system owing to the CAES unit. The proposed system in this manuscript turns the wood chips into syngas through the gasification process. The produced syngas is combusted in a BC to generate electricity. This is the common part of biomass power plants. The excess power in off-peak times is utilized for running the compressors of the CAES system. The stored compressed air is managed to discharge during peak periods to run the air turbine (AT). Also, the excess heat in different parts of the system is stored by pressurized water and thermal oil to exploit this energy in peak demand periods. The waste heat is also recovered by both RC and ORC units to generate more electricity during peak times. And finally, the residual heat of each stream is captured by water streams to produce domestic hot water (DHW). The mentioned stand-alone biomass power plant operates round the clock (8760 hr/year). The excess electricity at off-peak times (about 8 h) is stored by the CAES system and turns into electricity at peak demand periods (4 h). In peak periods the whole system operates in a full-load condition by producing electricity in different subsystems. Also during mid-peak times, the only unit that does the power generation is the BC. With this in mind, a detailed explanation of the system operation procedure in three different periods of peak, mid-peak, and off-peak is declared in the following sections.

2.1. System operation in mid-peak hours

During 12 h of the mid-peak electricity demand period, the only units that are under operation are biomass gasification and the BC. Based on Fig. 1, the biomass feedstock (stream 28) is mixed with the ambient air (stream 27). Through the gasification processes, a high-temperature synthesis gas (stream 29) is created, and the residual unreacted carbon so-called char is disposed from the gasifier. The ambient air (state 24) is compressed in the air compressor (AC_4) before entering the combustion chamber (CC). The compressed air (state 26) is mixed with syngas (state 29) and the flue gas (state 30) is produced by the complete combustion process in CC. The flue gas with high temperature and pressure expands in the gas turbine (GT) and then exchanges its heat with the inlet air of CC via Recuperator (Rec_2). Before getting into the FGC unit, the flue gas (state 32) releases its heat to the thermal oil stream (state 49). In FGC_1 the moisture content of the flue gas is condensed by the cold water stream (state 36) via FGC coils. Generally, there are two purposes for moisture absorption in FGC units: utilizing the latent heat of the vapor and preventing the corrosion of devices that can be caused by acidic solutions. The gathered water can be used as irrigation water in some special cases and circumstances (state 35). The residual content of the flue gas is exhausted to the environment (state 34) which is also essential for the photosynthesis of plants based on the existence of carbon dioxide (CO_2). Also, the cooling water in FGC which is heated by the flue gas stream is stored in the hot water tank (HWT_2).

2.2. System operation in off-peak hours

The stand-alone biomass plant is still operating under the same conditions as the mid-peak times. The only difference between these two periods is the charging process of the CAES system. Due to the lower electricity demand and consequently lower price in off-peak hours, a large portion of the generated power by GT is utilized to run the CAES compressors. The ambient air enters a three-stage compression unit with intercoolers (Intc) between each stage of compression. To minimize the required power of compression, three identical compressors with the same compression ratios are employed. Also, the heat of the compressed air stream is captured by pressurized water in each intercooler before entering the next compressor. This action significantly affects the power consumption of the compressors. At the last stage, the pressurized air is cooled down in the aftercooler (Aftc) and then is stored in the CAES tank. Finally, the hot pressurized water is stored in the HWT_1 for further applications in peak demand periods.

2.3. System operation in peak hours

During peak times, compressed air is discharged from the CAES tank. The regulation valve (Reg valve) controls the pressure fluctuations and sets the pressure on a specific value. The compressed air stream (state 9) is preheated by the outlet stream of hot pressurized water (stream 21) in the heat exchanger (Hx_1). The proposed stream at point 10 is heated in the Rec_1 by the outlet flue gas from the BC (stream 41) and then expands in the AT to the ambient pressure (state 12). The stored hot thermal oil in the hot oil tank (HOT) during mid-peak and off-peak times flows into the evaporators (Ev) of RC and ORC in peak demand periods. In the RC unit, the saturated water at state 62 is getting superheated by the Ev_1. The superheated vapor enters the steam turbine (ST) and expands to the ambient pressure at saturated vapor condition. The condensation process takes place in Con_1 and then the saturated water at state 61 is pressurized by the pump (P_2). Eventually, the pressurized water enters the Ev_1 to complete the cycle. At the following stages, the streams with a lower grade of thermal energy are employed to run the ORC unit. The residual heat of hot pressurized water (state 22), flue gas (state 42), and Thermiol VP1 at state 52 are utilized as the heat source of ORC. The operation procedure of ORC and RC are completely the same so it has been preferred to not repeat the same explanations in this part. Considering the outlet streams of Ev_2, the thermal oil stream gets into the Hx_3 to exchange its residual heat with a water stream to provide DHW. Then the mentioned oil stream is cooled down, depressurized, and stored in a cold oil tank (COT) and the oil's loop completes. Also, the flue gas stream enters the FGC_2 and experiences the same condensation process that was explained previously. The outlet of HWT_2 is divided into two streams. Stream 39 is employed as the coolant in the condenser (Con_1) to reduce the exergy destruction of Con_1. The outlet of Con_1 (state 40), streams 38, 23, 57, and 47 from the FGC_2 unit are mixed to provide a suitable temperature for DHW (state 58).

Table 1
Key design parameters of the proposed biomass-based CHP + CAES system [1,21,28–30].

Foundation parameter	Value	Unit
Ambient pressure	1.01	bar
Ambient temperature	298	K
Charging period	8	hr
Charging pressure	90	bar
Cold oil temperature	298	K
Coldwater temperature	293	K
Combustion chamber outlet temperature	1400	K
Compression ratio of BC air compressors	10	–
Compression ratio of CAES air compressors	4.467	–
Discharging period	4	hr
Discharging pressure	30	bar
Discount rate	7	%
Expansion ratio of air turbines	29.7	–
Expansion ratio of gas turbines	10	–
Expansion ratio of regulation valve	3	–
Gasifier operation pressure	1.01	bar
Gasifier operation temperature	1023	K
Interest rate	3	%
Isentropic efficiency of the air compressors	85	%
Isentropic efficiency of the air turbines	88	%
Isentropic efficiency of the gas turbines	90	%
Isentropic efficiency of the ORC turbines	80	%
Isentropic efficiency of the pumps	80	%
Isentropic efficiency of the steam turbines	90	%
Maintenance factor	6	%
Mass flow rate of BC input air	30	kg/s
Pinch-point temperature difference in the aftercooler	10	K
Pinch-point temperature difference in the evaporator	5	K
Pinch-point temperature difference in the flue gas condenser	5	K
Pinch-point temperature difference in the heat exchangers	5	K
Pinch-point temperature difference in the intercoolers	5	K
Pinch-point temperature difference in the ORC condenser	5	K
Pinch-point temperature difference in the Recuperators	10	K
Pinch-point temperature difference in the RC condenser	10	K
Price of off-peak electricity	0.09756	$/kWh
Price of on-peak electricity	0.12801	$/kWh
Purchase price of biomass feedstock	41	$/tonne
Purchase price of domestic hot water	0.015	$/gal
Purchase price of thermal oil	5000	$/tonne
System lifespan	20	years

Table 2
Ultimate composition analyses of dry wood [27].

Element	Mass fraction (wt %)
C	50
N	0
H	6
S	0
O	44

3. Modeling and formulation

The proposed system in this survey is analyzed from Energetic, Exergetic, Economic, Exergoeconomic, and Environmental perspectives. The mentioned analyses are accomplished to provide a clear and deep comprehension of the potentials of this system with different approaches. The simulation methodology and governing equations are expressed in this section. To simplify the modeling of the system, the following assumptions have been considered [22–27]:

- Pressure drops and heat losses besides kinetic and potential energies are neglected.
- The whole system operates in a steady-state condition.
- The isentropic efficiencies of pumps, air compressors, air turbines, gas turbines, ORC turbines, and steam turbines are 80%, 85%, 88%, 90%, 80%, and 90% respectively.
- The law of ideal gas mixture has been applied to syngas and flue gases due to high-temperature values in gasifier and combustion chamber.
- Wood chips with 20 wt% moisture content are considered as the feedstock of the gasifier.
- Tar formation in the gasification process is neglected and char is 100% unreacted carbon.
- The outlet streams of ORC and steam turbines are in saturated vapor condition.
- The outlet streams of condensers are in a saturated liquid state.
- The period of peak, mid-peak, and off-peak times are considered to be 4, 12, and 8 hours.

Other assumptions and key design conditions are listed in Table 1. It is worth mentioning that some of the design parameters (e.g. CAES vessel pressure, the mass flow rates of air, and feedstock) can be altered based on the load that the grid or the local community requires. Other design values like the prices of different components or the interest and discount rates are the average prices of the proposed products in the USA. Also, the designated pinch point differences or the isentropic efficiencies of different devices are based on the relevant published papers in the same field.

3.1. Energy analysis

In this part, energy analysis as a basic thermodynamic assessment is applied to different units of the system:

3.1.1. Gasification model

Biomass as a waste/low-cost fuel is converted to valuable products like gaseous or alcoholic fuels through a sequence of thermochemical reactions so-called gasification process [5]. In this study wood chips with 20 wt% moisture content is considered as the feedstock of the biomass gasification process. Generally, the chemical formula of the feedstock is $C_aH_bO_cN_d$ where a, b, c, and d subscripts represent the number of atoms for each element. Considering Table 2 and the mentioned formula for a single atom of carbon (a = 1), the other subscripts are obtained by the following equations:

$$b = \frac{H \cdot M_C}{C \cdot M_H}, c = \frac{O \cdot M_C}{C \cdot M_O}, d = \frac{N \cdot M_C}{C \cdot M_N} \quad (1)$$

Where H, O, N, C define the mass fraction of the feedstock and M_X denotes the molar mass of the elements.

The global gasification reaction in the gasifier that is utilized in this study is as follow [27]:

$$CH_bO_cN_d + \alpha H_2O + \beta(O_2 + 3.76N_2) \rightarrow x_1H_2 + x_2CO + x_3CO_2 + x_4H_2O + x_5CH_4 + x_6N_2 + \text{Char} \quad (2)$$

In this equation,α and β are representing the molar coefficient of water in wet biomass and the amount of required air per mole of feedstock respectively. Also, the molar coefficients of the product constituents are expressed by x_1 through x_6. The last product on the right side of the reaction is char (unreacted carbon) that is considered to be 15% of the total carbon in the feedstock. The molar coefficient of water in wet

Table 3
Energy rate and exergy rate balance equations for all system components [1,5,41–43].

component	Energy balance	Exergy destruction rate
Aftercooler	$\dot{Q}_{Aftc} = \dot{m}_6(h_6 - h_7) = \dot{m}_{16}(h_{19} - h_{16})$	$\dot{E}x^D_{Aftc} = t_{ch}\cdot\left(\dot{E}x_6 + \dot{E}x_{16} - \dot{E}x_7 - \dot{E}x_{19}\right)$
Air compressor 1	$\dot{W}_{AC_1} = \dot{m}_1(h_2 - h_1)$ $\eta_{AC_1} = (h_{2s} - h_1)/(h_2 - h_1)$	$\dot{E}x^D_{AC_1} = t_{ch}\cdot\left(\dot{E}x_1 + \dot{W}_{AC_1} - \dot{E}x_2\right)$
Air compressor 2	$\dot{W}_{AC_2} = \dot{m}_3(h_4 - h_3)$ $\eta_{AC_2} = (h_{4s} - h_3)/(h_4 - h_3)$	$\dot{E}x^D_{AC_2} = t_{ch}\cdot\left(\dot{E}x_3 + \dot{W}_{AC_2} - \dot{E}x_4\right)$
Air compressor 3	$\dot{W}_{AC_3} = \dot{m}_5(h_6 - h_5)$ $\eta_{AC_3} = (h_{6s} - h_5)/(h_6 - h_5)$	$\dot{E}x^D_{AC_3} = t_{ch}\cdot\left(\dot{E}x_5 + \dot{W}_{AC_3} - \dot{E}x_6\right)$
Air compressor 4	$\dot{W}_{AC_4} = \dot{m}_{24}(h_{25} - h_{24})$ $\eta_{AC_4} = (h_{25s} - h_{24})/(h_{25} - h_{24})$	$\dot{E}x^D_{AC_4} = 24\cdot\left(\dot{E}x_{24} + \dot{W}_{AC_4} - \dot{E}x_{25}\right)$
Air turbine	$\dot{W}_{AT} = \dot{m}_{11}(h_{11} - h_{12})$ $\eta_{AT} = (h_{11} - h_{12})/(h_{11} - h_{12s})$	$\dot{E}x^D_{AT} = t_{dch}\cdot\left(\dot{E}x_{11} - \dot{W}_{AT} - \dot{E}x_{12}\right)$
CAES tank	$h_7 = h_8$	$\dot{E}x^D_{CAES} = t_{ch}\cdot\dot{E}x_7 - t_{dch}\cdot\dot{E}x_8$
Combustion chamber	Eq. (18)	$\dot{E}x^D_{CC} = 24\cdot\left(\dot{E}x_{26} + \dot{E}x_{29} - \dot{E}x_{30}\right)$
Condenser 1	$\dot{Q}_{Con_1} = \dot{m}_{60}(h_{60} - h_{61}) = \dot{m}_{39}(h_{40} - h_{39})$	$\dot{E}x^D_{Con_1} = t_{dch}\cdot\left(\dot{E}x_{60} + \dot{E}x_{39} - \dot{E}x_{61} - \dot{E}x_{40}\right)$
Condenser 2	$\dot{Q}_{Con_2} = \dot{m}_{64}(h_{64} - h_{65}) = \dot{m}_{67}(h_{68} - h_{67})$	$\dot{E}x^D_{Con_2} = t_{dch}\cdot\left(\dot{E}x_{64} + \dot{E}x_{67} - \dot{E}x_{65} - \dot{E}x_{68}\right)$
Cold oil tank	$h_{55} = h_{48}$	$\dot{E}x^D_{COT} = t_{dch}\cdot\dot{E}x_{55} - (24 - t_{dch})\cdot\dot{E}x_{48}$
Evaporator 1	$\dot{Q}_{Ev_1} = \dot{m}_{51}(h_{51} - h_{52}) = \dot{m}_{62}h_{59} - h_{62})$	$\dot{E}x^D_{Ev_1} = t_{dch}\cdot\left(\dot{E}x_{51} + \dot{E}x_{62} - \dot{E}x_{52} - \dot{E}x_{59}\right)$
Evaporator 2	$\dot{Q}_{Ev_2} = \dot{m}_{22}(h_{22} - h_{23}) + \dot{m}_{42}(h_{42} - h_{43}) + \dot{m}_{52}(h_{52} - h_{53}) = \dot{m}_{66}(h_{63} - h_{66})$	$\dot{E}x^D_{Ev_2} = t_{dch}\cdot\left(\dot{E}x_{22} + \dot{E}x_{42} + \dot{E}x_{52} + \dot{E}x_{66} - \dot{E}x_{23} - \dot{E}x_{43} - \dot{E}x_{53} - \dot{E}x_{63}\right)$
Expansion valve	$h_{54} = h_{55}$	$\dot{E}x^D_{Valve} = t_{dch}\cdot\left(\dot{E}x_{54} - \dot{E}x_{55}\right)$
Flue gas condensation 1	$\dot{Q}_{FGC_1} = \dot{m}_{33}h_{33} - \dot{m}_{34}h_{34} - \dot{m}_{35}h_{35} = \dot{m}_{36}(h_{37} - h_{36})$	$\dot{E}x^D_{FGC_1} = (24 - t_{dch})\cdot\left(\dot{E}x_{33} + \dot{E}x_{36} - \dot{E}x_{34} - \dot{E}x_{35} - \dot{E}x_{37}\right)$
Flue gas condensation 2	$\dot{Q}_{FGC_2} = \dot{m}_{43}h_{43} - \dot{m}_{44}h_{44} - \dot{m}_{45}h_{45} = \dot{m}_{46}(h_{47} - h_{46})$	$\dot{E}x^D_{FGC_2} = t_{dch}\cdot\left(\dot{E}x_{43} + \dot{E}x_{46} - \dot{E}x_{44} - \dot{E}x_{45} - \dot{E}x_{47}\right)$
Gasifier	Eq. (12)	$\dot{E}x^D_{Gasifier} = 24\cdot\left(\dot{E}x_{27} + \dot{E}x_{28} - \dot{E}x_{29} - \dot{E}x_{Char}\right)$
Gas turbine	$\dot{W}_{GT} = \dot{m}_{30}(h_{30} - h_{31})$ $\eta_{GT} = (h_{30} - h_{31})/(h_{30} - h_{31s})$	$\dot{E}x^D_{GT} = 24\cdot\left(\dot{E}x_{30} - \dot{W}_{GT} - \dot{E}x_{31}\right)$
Heat exchanger 1	$\dot{Q}_{Hx_1} = \dot{m}_9(h_{10} - h_9) = \dot{m}_{21}(h_{21} - h_{22})$	$\dot{E}x^D_{Hx_1} = t_{dch}\cdot\left(\dot{E}x_9 + \dot{E}x_{21} - \dot{E}x_{10} - \dot{E}x_{22}\right)$
Heat exchanger 2	$\dot{Q}_{Hx_2} = \dot{m}_{32}(h_{32} - h_{33}) = \dot{m}_{49}(h_{50} - h_{49})$	$\dot{E}x^D_{Hx_2} = (24 - t_{dch})\cdot\left(\dot{E}x_{32} + \dot{E}x_{49} - \dot{E}x_{33} - \dot{E}x_{50}\right)$
Heat exchanger 3	$\dot{Q}_{Hx_3} = \dot{m}_{53}(h_{53} - h_{54}) = \dot{m}_{56}(h_{57} - h_{56})$	$\dot{E}x^D_{Hx_3} = t_{dch}\cdot\left(\dot{E}x_{53} + \dot{E}x_{56} - \dot{E}x_{54} - \dot{E}x_{57}\right)$
Hot oil tank	$h_{50} = h_{51}$	$\dot{E}x^D_{HOT} = (24 - t_{dch})\cdot\dot{E}x_{50} - t_{dch}\cdot\dot{E}x_{51}$
Hot water tank 1	$h_{20} = h_{21}$	$\dot{E}x^D_{HWT_1} = t_{ch}\cdot\dot{E}x_{20} - t_{dch}\cdot\dot{E}x_{21}$
Hot water tank 2	$h_{37} = h_{38} = h_{39}$	$\dot{E}x^D_{HWT_2} = (24 - t_{dch})\cdot\dot{E}x_{37} - t_{dch}\cdot\left(\dot{E}x_{38} + \dot{E}x_{39}\right)$
Intercooler 1	$\dot{Q}_{Intc_1} = \dot{m}_2(h_2 - h_3) = \dot{m}_{14}(h_{17} - h_{14})$	$\dot{E}x^D_{Intc_1} = t_{ch}\cdot\left(\dot{E}x_2 + \dot{E}x_{14} - \dot{E}x_3 - \dot{E}x_{17}\right)$
Intercooler 2	$\dot{Q}_{Intc_2} = \dot{m}_4(h_4 - h_5) = \dot{m}_{15}(h_{18} - h_{15})$	$\dot{E}x^D_{Intc_2} = t_{ch}\cdot\left(\dot{E}x_4 + \dot{E}x_{15} - \dot{E}x_5 - \dot{E}x_{18}\right)$
ORC turbine	$\dot{W}_{OT} = \dot{m}_{63}(h_{63} - h_{64})$ $\eta_{OT} = (h_{63} - h_{64})/(h_{63} - h_{64s})$	$\dot{E}x^D_{OT} = t_{dch}\cdot\left(\dot{E}x_{63} - \dot{W}_{OT} - \dot{E}x_{64}\right)$
Pump 1	$\dot{W}_{P_1} = \dot{m}_{48}(h_{49} - h_{48})$ $\eta_{P_1} = (h_{49s} - h_{48})/(h_{49} - h_{48})$	$\dot{E}x^D_{P_1} = (24 - t_{dch})\cdot\left(\dot{E}x_{48} + \dot{W}_{P_1} - \dot{E}x_{49}\right)$
Pump 2	$\dot{W}_{P_2} = \dot{m}_{61}(h_{62} - h_{61})$ $\eta_{P_2} = (h_{62s} - h_{61})/(h_{62} - h_{61})$	$\dot{E}x^D_{P_2} = t_{dch}\cdot\left(\dot{E}x_{61} + \dot{W}_{P_2} - \dot{E}x_{62}\right)$
Pump 3	$\dot{W}_{P_3} = \dot{m}_{65}(h_{66} - h_{65})$ $\eta_{P_3} = (h_{66s} - h_{65})/(h_{66} - h_{65})$	$\dot{E}x^D_{P_3} = t_{dch}\cdot\left(\dot{E}x_{65} + \dot{W}_{P_3} - \dot{E}x_{66}\right)$
Recuperator 1	$\dot{Q}_{Rec_1} = \dot{m}_{10}(h_{11} - h_{10}) = \dot{m}_{41}(h_{41} - h_{42})$	$\dot{E}x^D_{Rec_1} = t_{dch}\cdot\left(\dot{E}x_{41} + \dot{E}x_{10} - \dot{E}x_{11} - \dot{E}x_{42}\right)$
Recuperator 2	$\dot{Q}_{Rec_2} = \dot{m}_{25}(h_{26} - h_{25}) = \dot{m}_{31}(h_{31} - h_{32})$	$\dot{E}x^D_{Rec_2} = 24\cdot\left(\dot{E}x_{25} + \dot{E}x_{31} - \dot{E}x_{26} - \dot{E}x_{32}\right)$
Regulation valve	$h_8 = h_9$	$\dot{E}x^D_{\text{Reg valve}} = t_{dch}\cdot\left(\dot{E}x_8 - \dot{E}x_9\right)$
Steam turbine	$\dot{W}_{ST} = \dot{m}_{59}(h_{59} - h_{60})$ $\eta_{ST} = (h_{59} - h_{60})/(h_{59} - h_{60s})$	$\dot{E}x^D_{ST} = t_{dch}\cdot\left(\dot{E}x_{59} - \dot{W}_{ST} - \dot{E}x_{60}\right)$
Water pump	$\dot{W}_{WP} = \dot{m}_{13}(h_{14} - h_{13})$ $\eta_{WP} = (h_{14s} - h_{13})/(h_{14} - h_{13})$	$\dot{E}x^D_{WP} = t_{ch}\cdot\left(\dot{E}x_{13} + \dot{W}_{WP} - \dot{E}x_{14} - \dot{E}x_{15} - \dot{E}x_{16}\right)$

Table 4
Mass balance equations in different units of the system [19,30].

Unit	Mass balance equation
Gasifier + BC	$\dot{m}_{28}+\dot{m}_{27}=\dot{m}_{29}+\dot{m}_{Char},\ \dot{m}_{24}=\dot{m}_{25}=\dot{m}_{26},\ \dot{m}_{26}+\dot{m}_{29}=\dot{m}_{30}$ $\dot{m}_{30}=\dot{m}_{31}=\dot{m}_{32}$ or $\dot{m}_{41},\ \dot{m}_{32}=\dot{m}_{33},\ \dot{m}_{33}=\dot{m}_{34}+\dot{m}_{35}$ $\dot{m}_{41}=\dot{m}_{42}=\dot{m}_{43},\ \dot{m}_{43}=\dot{m}_{44}+\dot{m}_{45}$
CAES	$\dot{m}_1=\dot{m}_2=\dot{m}_3=\dot{m}_4=\dot{m}_5=\dot{m}_6=\dot{m}_7,\ \dot{m}_7\cdot t_{ch}=\dot{m}_8\cdot t_{dch}$
WHR	$\dot{m}_8=\dot{m}_9=\dot{m}_{10}=\dot{m}_{11}=\dot{m}_{12},\ \dot{m}_{13}=\dot{m}_{14}+\dot{m}_{15}+\dot{m}_{16},$ $\dot{m}_{14}=\dot{m}_{17},\ \dot{m}_{15}=\dot{m}_{18},\ \dot{m}_{16}=\dot{m}_{19},\ \dot{m}_{17}+\dot{m}_{18}+\dot{m}_{19}=\dot{m}_{20}$ $\dot{m}_{21}=\dot{m}_{22}=\dot{m}_{23},\ \dot{m}_{48}=\dot{m}_{49}=\dot{m}_{50},\ \dot{m}_{50}\cdot(24-t_{dch})=\dot{m}_{51}\cdot t_{dch}$ $\dot{m}_{51}=\dot{m}_{52}=\dot{m}_{53}=\dot{m}_{54}=\dot{m}_{55},\ \dot{m}_{55}\cdot t_{dch}=\dot{m}_{48}\cdot(24-t_{dch})$ $\dot{m}_{59}=\dot{m}_{60}=\dot{m}_{61}=\dot{m}_{62},\ \dot{m}_{63}=\dot{m}_{64}=\dot{m}_{65}=\dot{m}_{66},\ \dot{m}_{67}=\dot{m}_{68}$ $\dot{m}_{36}=\dot{m}_{37},\ \dot{m}_{37}\cdot(24-t_{dch})=(\dot{m}_{38}+\dot{m}_{39})\cdot t_{dch},\ \dot{m}_{39}=\dot{m}_{40}$ $\dot{m}_{46}=\dot{m}_{47},\ \dot{m}_{56}=\dot{m}_{57},\ \dot{m}_{23}+\dot{m}_{57}+\dot{m}_{47}+\dot{m}_{38}+\dot{m}_{40}=\dot{m}_{58}$

biomass (α) is calculated by [7]:

$$\alpha=\frac{M_{biomass}\cdot MC}{M_{water}\cdot(1-MC)},MC=\frac{\text{mass of water}}{\text{mass of wet biomass}}\times 100\% \tag{3}$$

Where MC is the moisture content in biomass feedstock. Also $M_{biomass}$ and M_{water} are the molar mass of biomass and water respectively.

There are 7 unknown variables (including x_1 through x_6 and β) in the proposed chemical reaction in Eq. (2), so 7 equations are required to solve the unknown variables. 4 equations are dedicated to carbon, hydrogen, nitrogen, and oxygen balances based on the proposed reaction in Eq. (2):

$$x_2+x_3+x_5+0.15=1 \quad \text{(Carbon balance)} \tag{4}$$

$$2\alpha+b=2x_1+2x_4+4x_5 \quad \text{(Hydrogen balance)} \tag{5}$$

$$\alpha+c+2\beta=x_2+2x_3+x_4 \quad \text{(Oxygen balance)} \tag{6}$$

$$3.76\beta=x_6 \quad \text{(Nitrogen balance)} \tag{7}$$

There are two other equations of the equilibrium constant for the formation of methane and shift reaction. These two constants are calculated as follow [31]:

$$k_1=\frac{x_5}{x_1^2} \tag{8}$$

$$k_2=\frac{x_1x_3}{x_2x_4} \tag{9}$$

Based on the gasification temperature these two equilibrium constants are obtained by [32]:

$$k_1=exp\left(\frac{7082.872}{T}-6.567\times lnT+\frac{7.466\times T}{2000}-\frac{2.164\times T^2}{6\times 10^6}+\frac{7.01\times 10^{-6}}{2\times T^2}+32.6055\right) \tag{10}$$

$$k_2=exp\left(\frac{5872.5}{T}+1.86\times lnT-2.69\times 10^{-4}\times T-\frac{58200}{T^2}-18.0131\right) \tag{11}$$

Considering the gasification as an adiabatic process, the energy balance equation will be the final equation to solve all 7 unknown variables [27]:

$$\begin{aligned}&\bar{h}^0_{f,wood}+\alpha\bar{h}^0_{f,H_2O}+3.76\beta\bar{h}^0_{f,N_2}+\beta\bar{h}^0_{f,O_2}=x_1\left(\bar{h}^0_{f,H_2}+\Delta\bar{h}_{H_2}\right)\\&+x_2\left(\bar{h}^0_{f,CO}+\Delta\bar{h}_{CO}\right)+x_3\left(\bar{h}^0_{f,CO_2}+\Delta\bar{h}_{CO_2}\right)+x_4\left(\bar{h}^0_{f,H_2O}+\Delta\bar{h}_{H_2O}\right)\\&+x_5\left(\bar{h}^0_{f,CH_4}+\Delta\bar{h}_{CH_4}\right)+x_6\left(\bar{h}^0_{f,N_2}+\Delta\bar{h}_{N_2}\right)+0.15\left(\bar{h}^0_{f,Char}+\Delta\bar{h}_{Char}\right)\end{aligned} \tag{12}$$

Table 5
The cost function for different components of the system [1,10,34,43,49].

Components	Capital cost function
Aftercooler	$Z_{Aftc}=12000\left(\frac{A_{Aftc}}{100}\right)^{0.6}$
Air compressors	$Z_{AC}=7900\left(\dot{W}[kW]\right)^{0.62}$
Air turbine	$Z_{AT}=1100\left(\dot{W}_{AT}[kW]\right)^{0.81}$
CAES tank	$Z_{CAES}=2(V_{CAES})\times 112.5$
Cold oil tank	$Z_{COT}=134.2\cdot(V_{COT})$
Combustion chamber	$Z_{CC}=\frac{N_1\cdot\dot{m}_{Air}}{N_2-0.98}(1+exp(N_3T_{CC}-N_4))$
Condenser	$N_1=46.08,N_2=0.995,N_3=0.018,N_4=26.4$ $Z_{Con}=8000\left(\frac{A_{Con}}{100}\right)^{0.6}$
Evaporator	$Z_{Ev}=16000\left(\frac{A_{Ev}}{100}\right)^{0.6}$
Expansion/ Regulation valve	$Z_{Valve}=114.5\cdot\dot{m}_{in}$
Flue gas condenser	$Z_{FGC}=130\left(\frac{A_{FGC}}{0.093}\right)^{0.78}$
Gasifier	$Z_{Gasifier}=1600\left(\dot{m}_{biomass}[kg/hr]\right)^{0.67}$
Gas turbine	$Z_{GT}=\frac{N_1\dot{m}_{in}(kg/s)}{N_2-\eta_{GT}}ln\left(\frac{P_{in}}{P_{out}}\right)(1+exp(N_3T_{in}(K)-N_4))$
Heat exchanger	$N_1=479.34,N_2=0.92,N_3=0.036,N_4=54.4$ $Z_{HX}=130\left(\frac{A_{HX}}{0.093}\right)^{0.78}$
Hot oil tank	$Z_{HOT}=423\cdot(V_{HOT})$
Hot water tank	$Z_{HWT}=4042\cdot(V_{HWT})^{0.506}$
Intercooler	$Z_{Intc}=12000\left(\frac{A_{Intc}}{100}\right)^{0.6}$
ORC turbine	$Z_{OT}=4750\left(\dot{W}_{OT}[kW]\right)^{0.75}$
Pump	$Z_P=2100\left(\frac{\dot{W}_P[kW]}{10}\right)^{0.26}\left(\frac{1-\eta_P}{\eta_P}\right)^{0.5}$
Recuperator	$Z_{Rec}=12000\left(\frac{A_{Rec}}{100}\right)^{0.6}$
Steam turbine	$Z_{ST}=6000\left(\dot{W}_{ST}[kW]\right)^{0.7}$

Where $\Delta\bar{h}$ is the enthalpy difference between the actual state and the standard temperature and pressure (STP) condition and $\bar{h}^0_f$ is the enthalpy of formation.

3.1.2. Brayton cycle

The produced syngas through the gasification process is supplied to the CC of the BC. The compressed air in AC_4 is preheated by Rec_2 and then enters the CC to start the combustion reaction which is as follow [33]:

$$\begin{aligned}&x_1H_2+x_2CO+x_3CO_2+x_4H_2O+x_5CH_4+x_6N_2+\\&B(O_2+3.76N_2)\rightarrow n_1H_2O+n_2CO_2+n_3N_2+n_4O_2\end{aligned} \tag{13}$$

Where x_1 through x_6 are verified from gasifier section. Therefore there are 5 unknown variables of B and n_1 through n_4, and 5 equations below to solve these variables [34]:

$$2x_1+2x_4+4x_5=2n_1 \quad \text{(H Balance)} \tag{14}$$

Table 6
Cost balance and auxiliary equations for different components of the system,

Component	Cost balance	Auxiliary equation
Aftercooler	$\dot{C}_6 + \dot{C}_{16} + \dot{Z}_{Aftc} = \dot{C}_7 + \dot{C}_{19}$	$c_6 = c_7$
Air compressor 1	$\dot{C}_1 + \dot{C}_{W,AC_1} + \dot{Z}_{AC_1} = \dot{C}_2$	$c_1 = 0,\ c_{w,AC_1} = c_{w,GT}$
Air compressor 2	$\dot{C}_3 + \dot{C}_{W,AC_2} + \dot{Z}_{AC_2} = \dot{C}_4$	$c_{w,AC_2} = c_{w,GT}$
Air compressor 3	$\dot{C}_5 + \dot{C}_{W,AC_3} + \dot{Z}_{AC_3} = \dot{C}_6$	$c_{w,AC_3} = c_{w,GT}$
Air compressor 4	$\dot{C}_{24} + \dot{C}_{W,AC_4} + \dot{Z}_{AC_4} = \dot{C}_{25}$	$c_{24} = 0,\ c_{w,AC_4} = c_{w,GT}$
Air turbine	$\dot{C}_{11} + \dot{Z}_{AT} = \dot{C}_{12} + \dot{C}_{W,AT}$	$c_{11} = c_{12}$
CAES tank	$\dot{C}_7 + \dot{Z}_{CAES} = \dot{C}_8$	
Combustion chamber	$\dot{C}_{26} + \dot{C}_{29} + \dot{Z}_{CC} = \dot{C}_{30}$	
Condenser 1	$\dot{C}_{39} + \dot{C}_{60} + \dot{Z}_{Con_1} = \dot{C}_{40} + \dot{C}_{61}$	$c_{60} = c_{61}$
Condenser 2	$\dot{C}_{64} + \dot{C}_{67} + \dot{Z}_{Con_2} = \dot{C}_{65} + \dot{C}_{68}$	$c_{64} = c_{65}$
Cold oil tank	$\dot{C}_{55} + \dot{Z}_{COT} = \dot{C}_{48}$	$c_{48} = 0$
Evaporator 1	$\dot{C}_{51} + \dot{C}_{62} + \dot{Z}_{Ev_1} = \dot{C}_{52} + \dot{C}_{59}$	$c_{51} = c_{52}$
Evaporator 2	$\dot{C}_{22} + \dot{C}_{42} + \dot{C}_{52} + \dot{C}_{66} + \dot{Z}_{Ev_2} = \dot{C}_{23} + \dot{C}_{43} + \dot{C}_{53} + \dot{C}_{63}$	$c_{22} = c_{23},\ c_{42} = c_{43},\ c_{52} = c_{53}$
Expansion valve	$\dot{C}_{54} + \dot{Z}_{Epv} = \dot{C}_{55}$	
Flue gas condensation 1	$\dot{C}_{33} + \dot{C}_{36} + \dot{Z}_{FGC_1} = \dot{C}_{34} + \dot{C}_{35} + \dot{C}_{37}$	$c_{33} = c_{34} = c_{35}$
Flue gas condensation 2	$\dot{C}_{43} + \dot{C}_{46} + \dot{Z}_{FGC_2} = \dot{C}_{44} + \dot{C}_{45} + \dot{C}_{47}$	$c_{43} = c_{44} = c_{45}$
Gasifier	$\dot{C}_{27} + \dot{C}_{28} + \dot{Z}_{Gasifier} = \dot{C}_{29} + \dot{C}_{Char}$	$c_{Char} = c_{28} = 2.621\ \$/\mathrm{GJ}$ $c_{27} = 0$
Gas turbine	$\dot{C}_{30} + \dot{Z}_{GT} = \dot{C}_{31} + \dot{C}_{W,GT}$	$c_{30} = c_{31}$
Heat exchanger 1	$\dot{C}_9 + \dot{C}_{21} + \dot{Z}_{Hx_1} = \dot{C}_{10} + \dot{C}_{22}$	$c_{21} = c_{22}$
Heat exchanger 2	$\dot{C}_{32} + \dot{C}_{49} + \dot{Z}_{Hx_2} = \dot{C}_{50} + \dot{C}_{33}$	$c_{32} = c_{33}$
Heat exchanger 3	$\dot{C}_{53} + \dot{C}_{56} + \dot{Z}_{Hx_3} = \dot{C}_{54} + \dot{C}_{57}$	$c_{53} = c_{54}$
Hot oil tank	$\dot{C}_{50} + \dot{Z}_{HOT} = \dot{C}_{51}$	
Hot water tank 1	$\dot{C}_{20} + \dot{Z}_{HWT_1} = \dot{C}_{21}$	
Hot water tank 2	$\dot{C}_{37} + \dot{Z}_{HWT_2} = \dot{C}_{38} + \dot{C}_{39}$	$c_{38} = c_{39}$
Intercooler 1	$\dot{C}_2 + \dot{C}_{14} + \dot{Z}_{Intc_1} = \dot{C}_3 + \dot{C}_{17}$	$c_2 = c_3$
Intercooler 2	$\dot{C}_4 + \dot{C}_{15} + \dot{Z}_{Intc_2} = \dot{C}_5 + \dot{C}_{18}$	$c_4 = c_5$
ORC turbine	$\dot{C}_{63} + \dot{Z}_{OT} = \dot{C}_{64} + \dot{C}_{W,OT}$	$c_{63} = c_{64}$
Pump 1	$\dot{C}_{48} + \dot{C}_{W,P_1} + \dot{Z}_{P_1} + \dot{Z}_{Oil} = \dot{C}_{49}$	$c_{w,P_1} = c_{w,GT}$
Pump 2	$\dot{C}_{61} + \dot{C}_{W,P_2} + \dot{Z}_{P_2} = \dot{C}_{62}$	$c_{w,P_2} = c_{w,ST}$
Pump 3	$\dot{C}_{65} + \dot{C}_{W,P_3} + \dot{Z}_{P_3} = \dot{C}_{66}$	$c_{w,P_3} = c_{w,OT}$
Recuperator 1	$\dot{C}_{10} + \dot{C}_{41} + \dot{Z}_{Rec_1} = \dot{C}_{11} + \dot{C}_{42}$	$c_{41} = c_{42}$
Recuperator 2	$\dot{C}_{25} + \dot{C}_{31} + \dot{Z}_{Rec_2} = \dot{C}_{26} + \dot{C}_{32}$	$c_{31} = c_{32},\ c_{31} = c_{41}$
Regulation valve	$\dot{C}_8 + \dot{Z}_{\mathrm{Reg\ valve}} = \dot{C}_9$	
Steam turbine	$\dot{C}_{59} + \dot{Z}_{ST} = \dot{C}_{60} + \dot{C}_{W,ST}$	$c_{59} = c_{60}$
Water pump	$\dot{C}_{13} + \dot{C}_{W,WP} + \dot{Z}_{WP} = \dot{C}_{14} + \dot{C}_{15} + \dot{C}_{16}$	$c_{13} = 0,\ c_{w,WP} = c_{w,GT},\ c_{14} = c_{15} = c_{16}$

Table 7
Validation of gasification model with experimental results (considering wood chips as biomass feedstock with 20% moisture content at 800 ℃ gasification temperature) [54].

Composition	Model (%)	Experimental (%)
Carbon dioxide (CO_2)	14.18	16.42
Carbon monoxide (CO)	19.39	23.04
Hydrogen (H_2)	18.73	15.23
Methane (CH_4)	0.59	1.58
Nitrogen (N_2)	47.11	42.31
Oxygen (O_2)	0	1.42

$$x_2 + x_3 + x_5 = n_2 \quad (\mathrm{C\ Balance}) \tag{15}$$

$$x_2 + 2x_3 + x_4 + 2B = n_1 + 2n_2 + 2n_4 \quad (\mathrm{O\ \ Balance}) \tag{16}$$

$$x_6 + 3.76B = n_3 \quad (\mathrm{N_2\ \ Balance}) \tag{17}$$

Table 8
Verification of different units of the proposed system with related publications.

Unit	Parameter	Model	Reference	Error (%)
CAES [15]	Charging mass flow rate (kg/s)	1.49	1.50	0.67
	Volume of CAES tank (m^3)	3116.6	3074	1.38
	Consumed power by ACs (kW)	519.01	552	5.97
BC [34]	Mass flow rate of air (kg/s)	2.475	2.475	0.00
	Mass flow rate of fuel (kg/s)	0.569	0.624	8.81
	Exergy destruction of CC (kW)	793.6	850.8	6.72
RC [55]	Mass flow rate (kg/s)	2.312	2.312	0.00
	Inlet pressure of ST (bar)	18.76	19.96	6.01
	Generated power by ST (kW)	1493	1506	0.86
ORC [18]	Generated power by OT (kW)	111.68	110.2	1.34
	Mass flow rate (kg/s)	1.3200	1.270	3.94
	Waste heat recovery (kW)	442.57	433.2	2.16

Table 9
Thermodynamic and thermoeconomic properties of system streams.

State	Fluid	T (K)	P (bar)	h (kJ/kg)	s $(kJ/kg{\cdot}K)$	$\dot{m}$ (kg/s)	$\dot{E}x$ (kW)	$\dot{C}$ $(\$/hr)$	c $(\$/GJ)$
1	Air	298.0	1.01	424.29	3.88091	18.996	0.0000	0.000	0.000
2	Air	483.0	4.50	611.66	3.94082	18.996	3220.2	131.0	11.30
3	Air	298.0	4.50	423.49	3.44990	18.996	2424.7	98.68	11.30
4	Air	484.9	20.2	612.79	3.51018	18.996	5679.3	230.9	11.29
5	Air	298.0	20.2	419.96	3.00788	18.996	4859.8	197.6	11.29
6	Air	485.0	90.0	609.80	3.06827	18.996	8124.0	330.1	11.28
7	Air	303.0	90.0	411.43	2.55424	18.996	7265.7	295.2	11.28
8	Air	303.0	90.0	411.43	2.55424	37.991	14,531	341.3	6.524
9	Air	291.9	30.0	411.43	2.86648	37.991	10,996	341.5	8.627
10	Air	428.2	30.0	553.38	3.26572	37.991	11,869	384.5	8.998
11	Air	674.3	30.0	812.46	3.74308	37.991	16,308	485.5	8.271
12	Air	310.7	1.01	437.09	3.92298	37.991	10.100	0.301	8.271
13	Water	293.0	1.01	83.380	0.29432	14.670	0.0000	0.000	0.000
14	Water	293.0	15.5	84.750	0.29402	4.8030	7.0000	0.232	9.219
15	Water	293.0	15.5	84.750	0.29402	4.8650	7.1000	0.235	9.219
16	Water	293.0	15.5	84.750	0.29402	5.0030	7.3000	0.242	9.219
17	Water	468.0	15.5	829.00	2.28108	4.8030	785.30	33.27	11.77
18	Water	469.9	15.5	837.70	2.29964	4.8650	811.30	34.23	11.72
19	Water	470.0	15.5	837.97	2.30046	5.0030	834.40	35.69	11.88
20	Water	469.3	15.5	834.95	2.29377	14.670	2431.3	103.2	11.79
21	Water	469.3	15.5	834.95	2.29377	29.340	4862.6	106.3	6.071
22	Water	427.4	15.5	651.14	1.88362	29.340	2995.6	65.47	6.071
23	Water	354.8	15.5	343.16	1.09421	29.340	745.60	16.29	6.071
24	Air	298.0	1.01	424.29	3.88091	30.000	0.0000	0.000	0.000
25	Air	617.4	10.1	751.71	3.96361	30.000	9083.4	264.8	7.660
26	Air	866.0	10.1	1021.8	4.33067	30.000	14,038	373.3	6.970
27	Air	298.0	1.01	424.29	3.88091	4.2220	18.800	0.000	0.000
28	Biomass	298.0	1.01	N/A	N/A	2.2830	48,002	452.9	2.621
29	Syngas	1023	1.01	1705.9	8.40609	6.3400	27,635	409.6	4.117
30	Flue gas	1400	10.1	1713.0	7.74779	36.340	36,242	785.1	6.017
31	Flue gas	876.7	1.01	1065.0	7.83512	36.340	11,745	254.4	6.017
32	Flue gas	684.3	1.01	842.01	7.54856	36.340	6746.2	146.1	6.017
33	Flue gas	343.0	1.01	470.45	6.80146	36.340	1334.1	28.90	6.017
34	Exhaust gas	313.1	1.01	321.67	6.32904	34.682	758.20	16.42	6.017
35	Water	313.1	1.01	167.23	0.57143	1.6580	13.600	0.294	6.017
36	Water	293.0	1.01	83.380	0.29432	64.578	0.0000	0.000	0.000
37	Water	312.0	1.01	162.81	0.55699	64.578	159.40	13.20	23.00
38	Water	312.0	1.01	162.81	0.55699	150.24	370.90	7.940	5.946
39	Water	312.0	1.01	162.81	0.55699	172.65	426.20	9.124	5.946
40	Water	363.0	1.01	376.43	1.19111	172.65	5230.5	83.43	4.431
41	Flue gas	684.3	1.01	842.01	7.54856	36.340	6746.2	146.1	6.017
42	Flue gas	438.2	1.01	571.16	7.06050	36.340	2188.8	47.41	6.017
43	Flue gas	351.0	1.01	478.93	6.82577	36.340	1379.1	29.87	6.017
44	Exhaust gas	313.1	1.01	321.67	6.32904	34.682	758.20	16.42	6.017
45	Water	313.1	1.01	167.23	0.57143	1.6580	13.600	0.294	6.017
46	Water	293.0	1.01	83.380	0.29432	64.940	0.0000	0.000	0.000
47	Water	313.0	1.01	167.11	0.57076	64.940	177.80	18.06	28.22
48	TVP1	298.0	1.01	7.5200	0.02544	17.854	0.0000	0.000	0.000
49	TVP1	298.3	9.73	8.5500	0.02613	17.854	14.700	54.18	1025
50	TVP1	664.3	9.73	764.84	1.62808	17.854	4994.3	173.3	9.638
51	TVP1	664.3	9.73	764.84	1.62808	89.268	24,971	181.0	2.013
52	TVP1	438.2	9.73	254.96	0.69869	89.268	4178.5	30.28	2.013
53	TVP1	349.7	9.73	92.640	0.28593	89.268	669.00	4.848	2.013
54	TVP1	298.0	9.73	8.1500	0.02478	89.268	73.400	0.532	2.013
55	TVP1	298.0	1.01	8.1500	0.02754	89.268	0.0000	0.000	0.000
56	Water	293.0	1.01	83.380	0.29432	36.069	0.0000	0.000	0.000
57	Water	343.0	1.01	292.49	0.95326	36.069	578.80	25.99	12.47
58	Water	336.9	1.01	266.79	0.87766	453.24	5664.7	151.7	7.440
59	Water	649.3	14.6	3205.5	7.20547	16.343	17,931	163.1	2.526
60	Water	373.0	1.01	2675.4	7.35551	16.343	8548.8	77.75	2.526
61	Water	373.0	1.01	418.68	1.30590	16.343	635.80	5.783	2.526
62	Water	373.2	14.6	420.45	1.30686	16.343	660.30	7.037	2.960
63	ammonia	417.4	57.5	1812.1	5.59204	20.387	11,503	252.8	6.104
64	ammonia	303.0	11.6	1629.2	5.73638	20.387	6897.8	151.6	6.104
65	ammonia	303.0	11.6	484.19	1.95729	20.387	6512.5	143.1	6.104
66	ammonia	304.7	57.5	493.79	1.96360	20.387	6670.0	156.5	6.519
67	Water	293.0	1.01	83.380	0.29432	1116.3	0.0000	0.000	0.000
68	Water	298.0	1.01	104.29	0.36510	1116.3	196.90	12.50	17.63

Table 10
Significant results of the biomass-based CHP + CAES system.

Parameter	Unit	Value	Parameter	Unit	Value
$\dot{W}_{AC_1}$	kW	3559.4	$\dot{Q}_{biomass}$	kW	45,590
$\dot{W}_{AC_2}$	kW	3595.9	$\dot{Q}_{DHW}$	kW	83,131
$\dot{W}_{AC_3}$	kW	3606.1	T_{DHW}	K	336.9
$\dot{W}_{AC_4}$	kW	9822.8	$HHV_{Biomass}$	kJ/kg	19,970
$\dot{W}_{AT}$	kW	14,261	$LHV_{Biomass}$	kJ/kg	18,187
$\dot{W}_{GT}$	kW	23,551	LHV_{Syngas}	kJ/kg	3884.2
$\dot{W}_{OT}$	kW	3728.7	λ	–	1.1562
$\dot{W}_{ST}$	kW	8663.9	$ASED$	MJ/m^3	25.532
$\dot{W}_{P_1}$	kW	18.348	V_{HOT}	m^3	1814.7
$\dot{W}_{P_2}$	kW	29.001	V_{COT}	m^3	1212.3
$\dot{W}_{P_3}$	kW	195.81	V_{DHW}	m^3	6651.4
$\dot{W}_{WP}$	kW	26.715	V_{HWT_1}	m^3	486.07
W_{net}	MWh	348.34	V_{HWT_2}	m^3	4684.1
$\dot{Q}_{Intc_1}$	kW	3574.5	V_{CAES}	m^3	8049.2
$\dot{Q}_{Intc_2}$	kW	3662.9	Ex^D_{tot}	MWh	615.67
$\dot{Q}_{Aftc}$	kW	3768.1	$\dot{C}^D_{tot}$	$/hr	612.71
$\dot{Q}_{FGC_1}$	kW	5129.5	$\dot{Z}_{tot}$	$/hr	974.29
$\dot{Q}_{FGC_2}$	kW	5437.7	$\dot{C}_{tot}$	$/hr	1427.3
$\dot{Q}_{Hx_1}$	kW	5392.9	Profit	M$	180.79
$\dot{Q}_{Hx_2}$	kW	13,502	PP	year	2.068
$\dot{Q}_{Hx_3}$	kW	7542.1	CRF	–	0.0672
$\dot{Q}_{Rec_1}$	kW	9842.8	$SUCP$	$/GJ	6.7385
$\dot{Q}_{Rec_2}$	kW	8102.6	$LCOE$	$/GJ	13.508
$\dot{Q}_{Ev_1}$	kW	45,516	RTE_{tot}	%	70.86
$\dot{Q}_{Ev_2}$	kW	26,878	$ERTE_{tot}$	%	48.47
$\dot{Q}_{Con_1}$	kW	36,882	RTE_{Elec}	%	47.4
$\dot{Q}_{Con_2}$	kW	23,345	$RTE_{\text{stand-alone}}$	%	42.5

$$x_1\left(\overline{h}^0_{f,H_2}+\Delta\overline{h}_{H_2}\right)+x_2\left(\overline{h}^0_{f,CO}+\Delta\overline{h}_{CO}\right)+x_3\left(\overline{h}^0_{f,CO_2}+\Delta\overline{h}_{CO_2}\right)$$
$$+x_4\left(\overline{h}^0_{f,H_2O}+\Delta\overline{h}_{H_2O}\right)+x_5\left(\overline{h}^0_{f,CH_4}+\Delta\overline{h}_{CH_4}\right)+x_6\left(\overline{h}^0_{f,N_2}+\Delta\overline{h}_{N_2}\right)\quad\text{(Energy Balance)}$$
$$+3.76B\overline{h}^0_{f,N_2}+B\overline{h}^0_{f,O_2}=n_1\left(\overline{h}^0_{f,H_2O}+\Delta\overline{h}_{H_2O}\right)+n_2\left(\overline{h}^0_{f,CO_2}+\Delta\overline{h}_{CO_2}\right)$$
$$+n_3\left(\overline{h}^0_{f,N_2}+\Delta\overline{h}_{N_2}\right)+n_4\left(\overline{h}^0_{f,O_2}+\Delta\overline{h}_{O_2}\right)\quad(18)$$

The isentropic efficiency and consumed power by all types of turbines can be calculated as below [35]:

$$\eta_T=\frac{h_{in}-h_{out}}{h_{in}-h_{out,s}}\quad(19)$$

$$\dot{W}_T=\dot{m}_{in}(h_{in}-h_{out})\quad(20)$$

The subscripts *in*,*out* and *s* are respectively dedicated to inlet/outlet streams and the isentropic state.

The energy balance equations of other devices and units (including heat exchangers, evaporators, condensers, etc.) are listed in Table 3. Also, the mass balance equations are presented in Table 4.

3.1.3. CAES system

The excess generated power by the stand-alone biomass power plant is utilized for charging the CAES system. Three identical ACs with the same compression ratios are employed to produce compressed air in off-peak periods. The isentropic efficiency and power consumption of each AC are defined by [36]:

$$\eta_{AC}=\frac{h_{out,s}-h_{in}}{h_{out}-h_{in}}\quad(21)$$

$$\dot{W}_{AC}=\dot{m}_{in}(h_{out}-h_{in})\quad(22)$$

The consumed power and the isentropic efficiency of the pumps are [24]:

$$\dot{W}_P=\dot{m}_{in}(h_{out}-h_{in})\quad(23)$$

$$\eta_P=\frac{h_{out,s}-h_{in}}{h_{out}-h_{in}}\quad(24)$$

Also, the volume of the CAES tank and other thermal storage tanks are calculated by [4]:

$$V_{CAES}=\frac{\dot{m}_7\cdot t_{ch}\cdot 3600}{\rho_7-\rho_9}=\frac{\dot{m}_8\cdot t_{dch}\cdot 3600}{\rho_7-\rho_9}\quad(25)$$

$$V_{\text{Tanks}}=\frac{\dot{m}_{in}\cdot t_{in}\cdot 3600}{\rho_{in}}=\frac{\dot{m}_{out}\cdot t_{out}\cdot 3600}{\rho_{out}}\quad(26)$$

Based on Eq. (26), t_{in} and t_{out} are representing the time of charging and discharging processes of each tank.

3.1.4. WHR units

Thermal storage units beside RC, ORC, and FGC are the cascade WHR units of this system. The operation procedure of RC and ORC are almost the same and the related equations of each component are proposed in different sections. The other energy and mass balance equations are listed in Tables 3, 4 respectively.

3.2. Exergy analysis

Due to the dependency of exergy on the environmental condition, this evaluation is a complementary method for energy analysis. Exergy assessment also determines the maximum available work in a process and provides a proper connection between the system performance and the environment. The exergy rate balance for each component can be calculated as follow [37]:

$$\dot{E}x_Q+\sum\dot{E}x_{in}=\sum\dot{E}x_{out}+\dot{E}x_W+\dot{E}x^D,\dot{E}x_W=\dot{W},\dot{E}x_Q=\dot{Q}_j\left(1-\frac{T_0}{T_j}\right)\quad(27)$$

Where the subscripts *j* and 0 are dedicated to the state number and the dead state condition.

Generally, exergy consists of four main categories of physical, chemical, kinetic, and potential. Where the last two are neglected based on the low velocity and elevation. So the exergy rate is expressed as [38]:

$$\dot{E}x=\dot{E}x_{ph}+\dot{E}x_{Ch}\quad(28)$$

And the physical exergy rate is [39]:

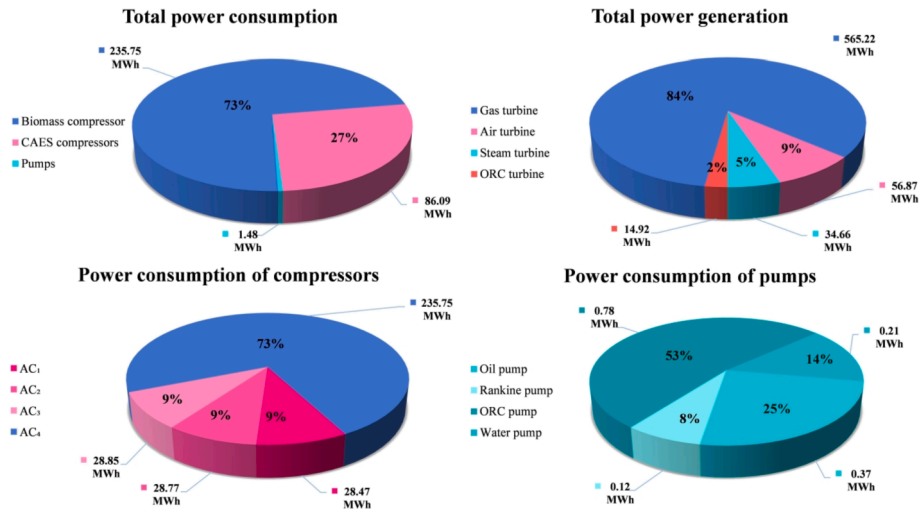

Fig. 2. The share of power consumption/generation for different subsystems and components.

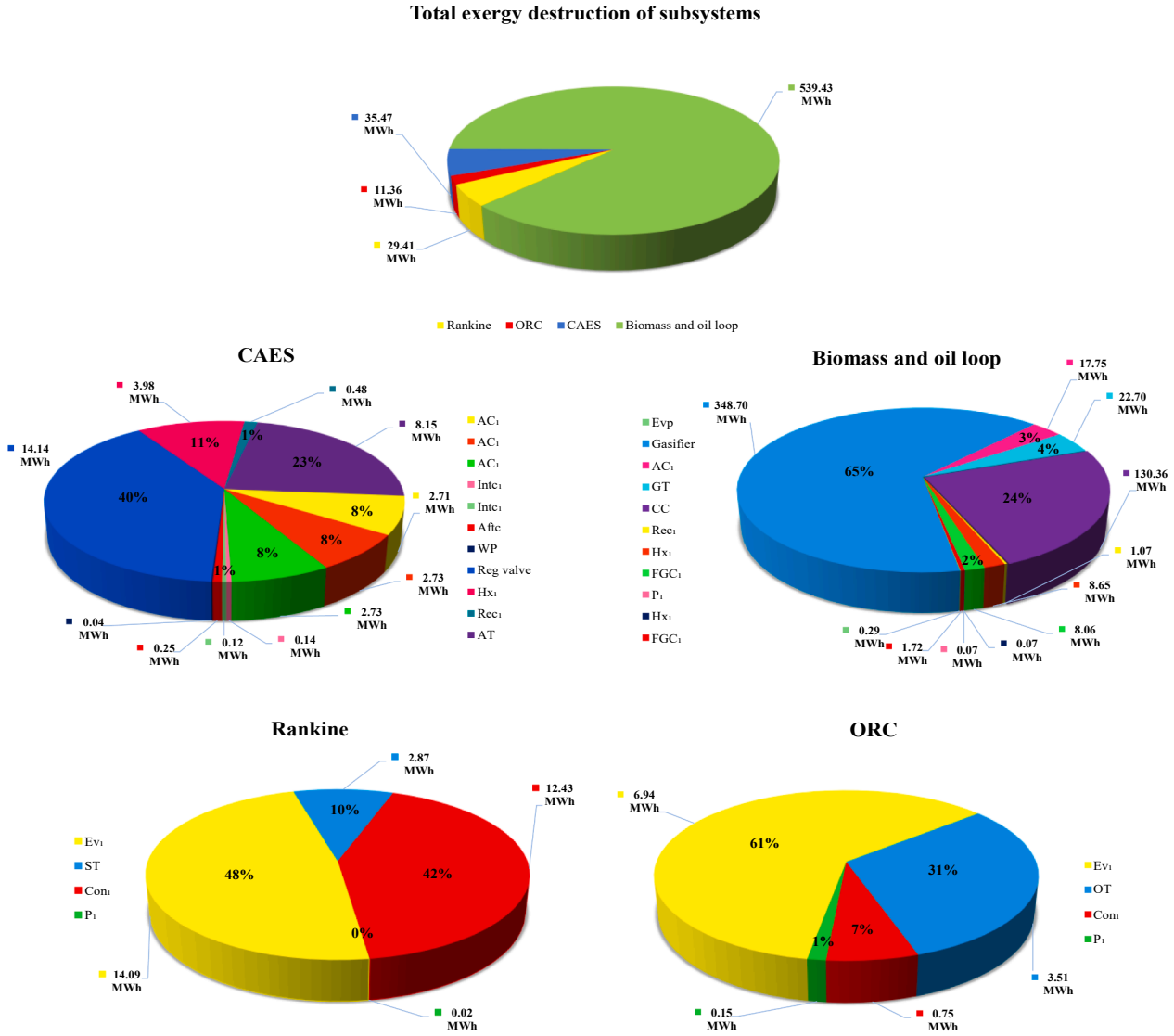

Fig. 3. The portion of exergy destruction for different subsystems and components.

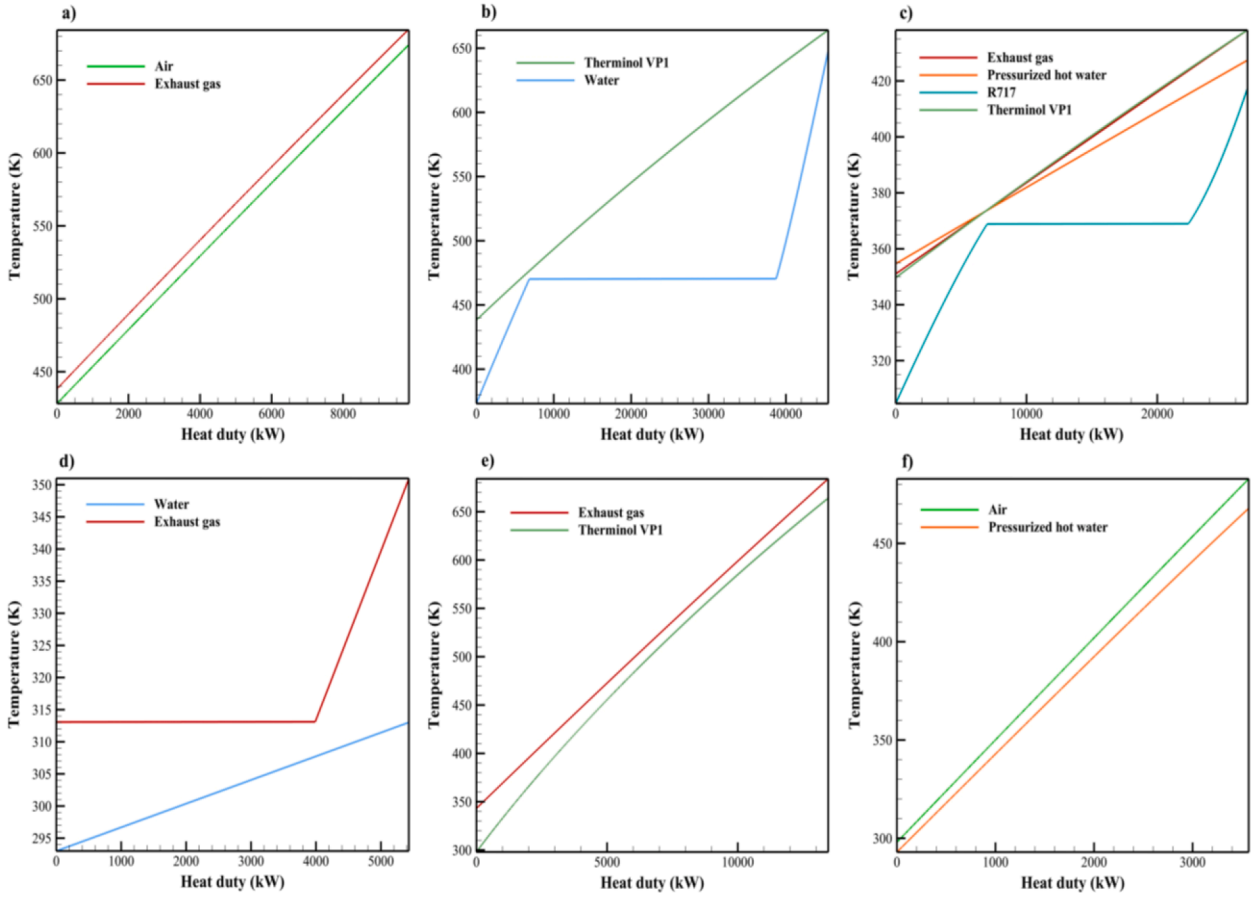

Fig. 4. Composite curves of some of the critical heat exchangers of the system: a) Rec_1, b) Ev_1, c) Ev_2, d) FGC_2, e) Hx_2, f) $Intc_1$.

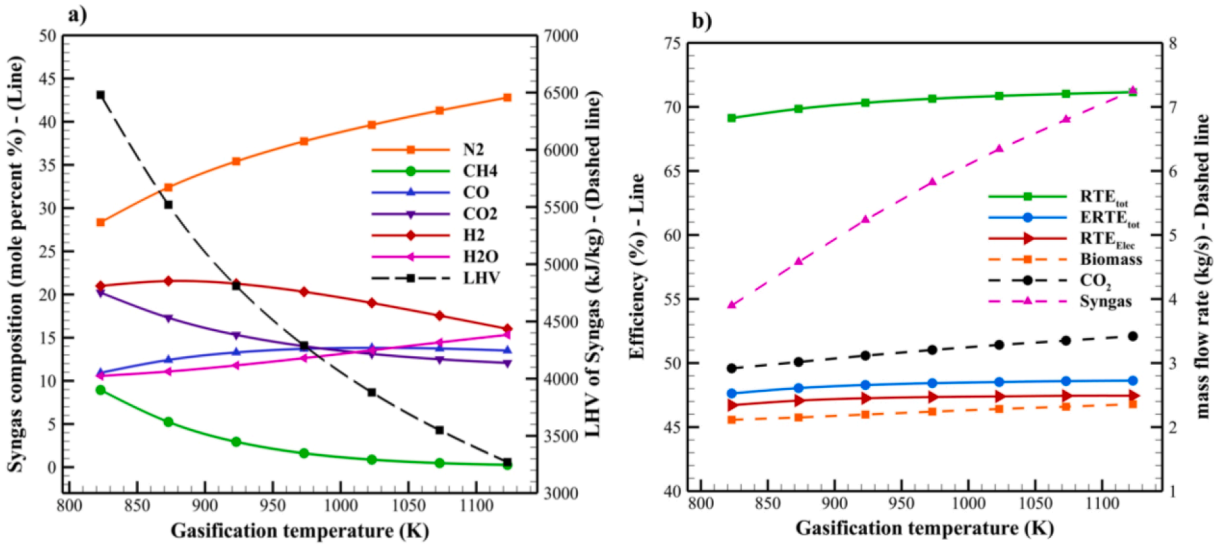

Fig. 5. The effect of gasification temperature on a) Syngas compositions and LHV value b) The overall efficiencies and mass flue rate of biomass, syngas, and CO_2.

$$\dot{E}x_{ph} = \dot{m}_j\left(\left(h_j - h_0\right) - T_0\left(s_j - s_0\right)\right) \tag{29}$$

The molar chemical exergy for the ideal gas mixture and the exergy rate of biomass is calculated by [40]:

$$\overline{ex}_{Ch} = \sum_n f_n \overline{ex}^n_{Ch} + RT_0 \sum_n f_n ln(f_n) \tag{30}$$

$$\dot{E}x_{Biomass} = \dot{m}_{Biomass} \cdot \lambda \cdot LHV_{Biomass} \tag{31}$$

Where f_n indicates the molar fraction of n^{th} element, R is the universal gas constant, and $\overline{ex}^n_{ch}$ is the standard exergy of each component. Also, the coefficient λ is as follow [40]:

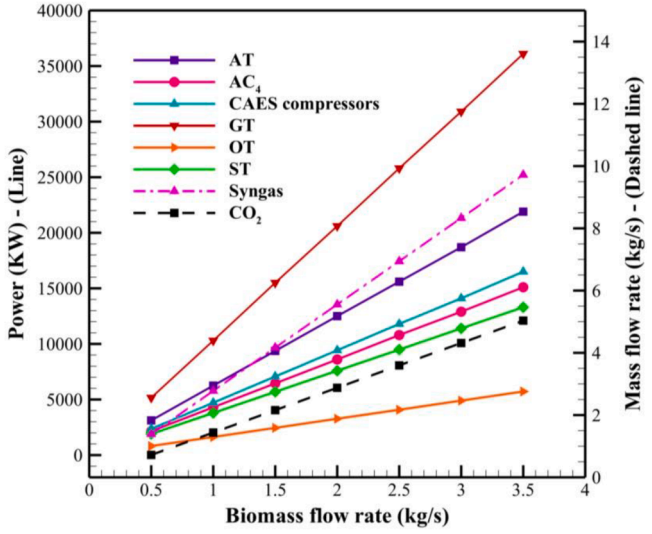

Fig. 6. The impact of feedstock flow rate on power generation/consumption different units and mass flow rate of syngas and CO_2.

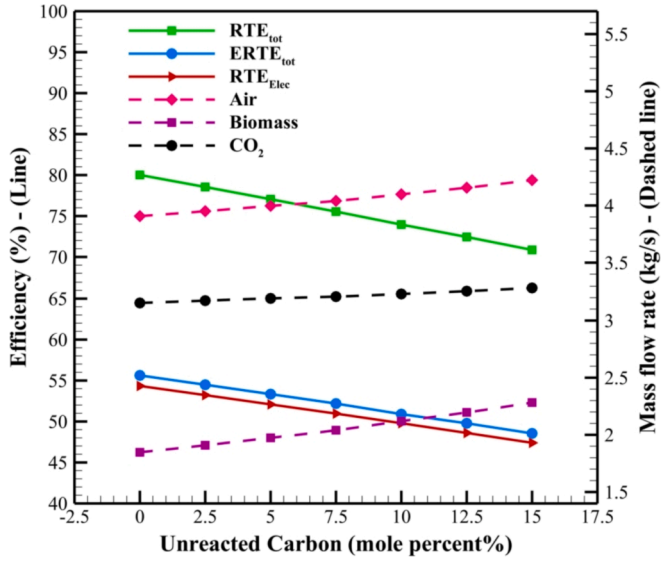

Fig. 7. The effect of unreacted carbon percentage on overall performance criteria and mass flow rate of gasifier's feedstocks and emitted CO_2.

$$\lambda = \frac{1.044 + 0.016\left(\frac{H}{C}\right) - 0.3493\left(\frac{O}{C}\right)\left[1 + 0.0531\left(\frac{H}{C}\right)\right] + 0.0493\left(\frac{N}{C}\right)}{1 - 0.4124\left(\frac{O}{C}\right)} \tag{32}$$

Alongside the energy balance equations, the exergy destruction rate of different components is presented in Table 3.

3.3. Exergoeconomic analysis

The exergoeconomic analysis is a great tool that provides a comprehensive prospect of the economic issues of a system while considering the exergetic perspective. These calculations aim to figure out the cost rate of each stream and consequently the value of the products of the system. Through this assessment, the cost balance equations are applied to each component of the system as follow [43]:

$$\sum \dot{C}_{out,k} + \dot{C}_{W,k} = \sum \dot{C}_{in,k} + \dot{C}_{Q,k} + \dot{Z}_k, \dot{C} = c \cdot \dot{E}x \tag{33}$$

Here c represents the cost per exergy unit and $\dot{C}$ indicates the cost rate for inlet/outlet streams or the generated power and received thermal energy by the k^{th} unit.

The presented cost functions (Z_k) in Table 5 is also converted to a cost rate by the following equation [43]:

$$\dot{Z}_k = \frac{Z_k \cdot CRF \cdot \phi}{\tau} \tag{34}$$

Where τ and ϕ are respectively dedicated to the annual operating hours and maintenance factor of each component. The capital recovery factor (CRF) is also calculated as follow [44]:

$$CRF = \frac{i(1+i)^n}{(1+i)^n - 1} \tag{35}$$

Where n and i are respectively indicating the service year and the interest rate of the case study.

It must be indicated here that the proposed cost functions in Table 5 have different reference years. Therefore the Marshal and Swift (M&S) factor has been multiplied in each cost function to convert it to a present cost as follow [10]:

$$\text{Cost at present year} = \text{Cost at reference year} \times \frac{M\&S \text{ index for the present year}}{M\&S \text{ index at the reference year}} \tag{36}$$

Generally, solving the cost balance equations for some units with more than one product needs auxiliary equations. Table 6 represents the cost balance and auxiliary equations of different components. Also, the average cost of fuel and product which are consumed or produced in each component is calculated by the division of cost rates to the exergy rates as follow [44]:

$$c_k^f = \frac{\dot{C}_k^f}{3.6 \times \dot{E}x_k^f} \times 10^3 \tag{37}$$

$$c_k^p = \frac{\dot{C}_k^p}{3.6 \times \dot{E}x_k^p} \times 10^3 \tag{38}$$

The cost rate of destruction in each component is also expressed as the equation below [45]:

$$\dot{C}_k^D = 3.6 \times 10^{-3} \times c_k^f \cdot \dot{E}x_k^D \tag{39}$$

Relative cost difference and Exergoeconomic factors are also determined by the following equations [46]:

$$r_k = \frac{c_k^p - c_k^f}{c_k^f} \tag{40}$$

$$f_k = \frac{\dot{Z}_k}{\dot{Z}_k + \dot{C}_k^D} \tag{41}$$

To evaluate the total performance of different energy systems in terms of thermoeconomic analysis the following parameters are calculated [47,48]:

$$\dot{C}_{tot} = \left(\dot{Z}_{tot} + \dot{C}_{Biomass} + \dot{C}_{CO_2}\right), \dot{Z}_{tot} = \sum_{k=1}^{n} \dot{Z}_k, \tag{42}$$

$$SUCP = \frac{\dot{C}_{net}^W + \dot{C}_{58}}{\dot{W}_{net} + \dot{E}x_{58}}, \dot{C}_{net}^W = \dot{C}_{\text{Generation}}^W - \dot{C}_{\text{Consumption}}^W \tag{43}$$

$$LCOE = \frac{\dot{C}_{tot}}{\dot{W}_{net}} \tag{44}$$

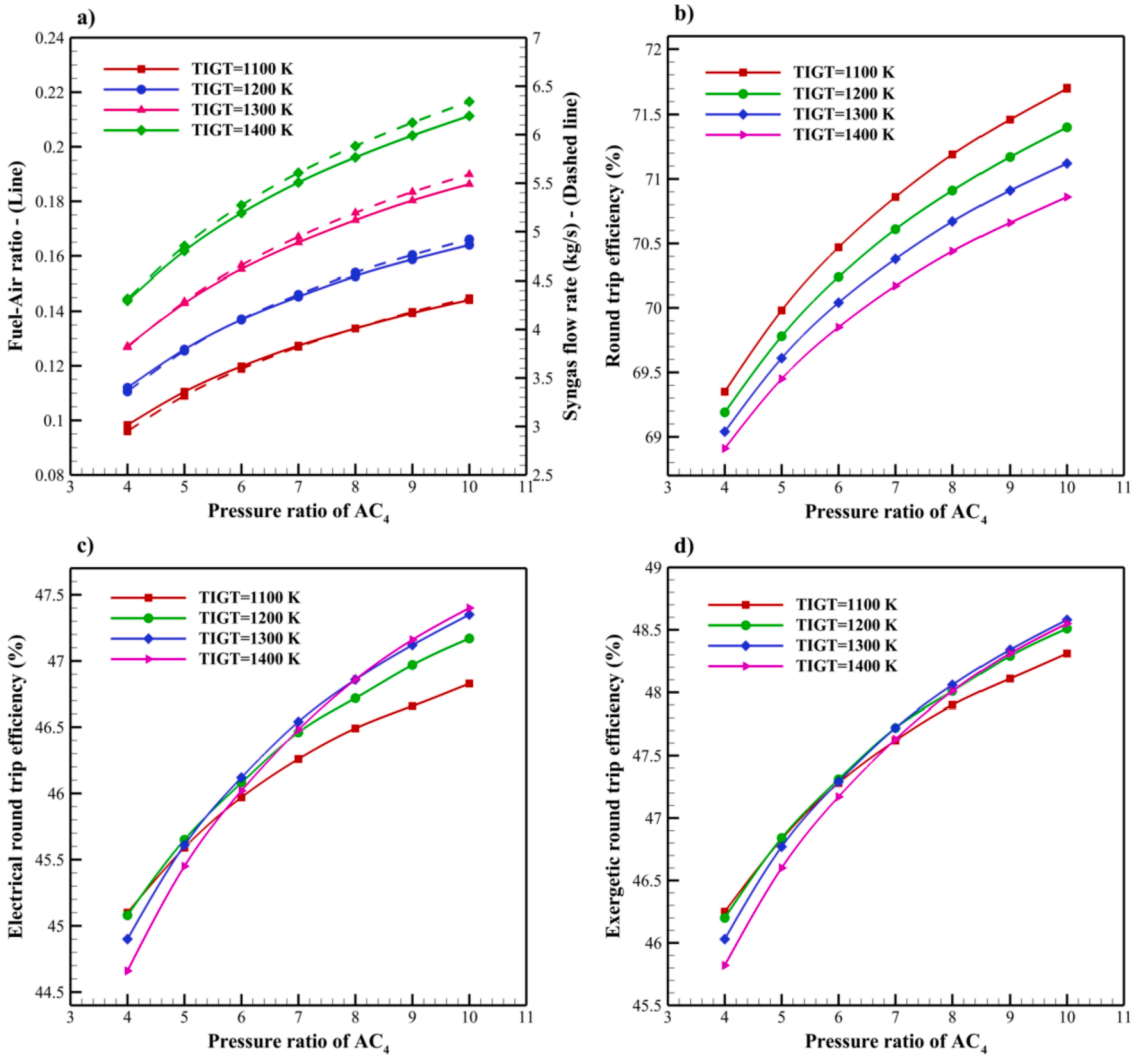

Fig. 8. The influence of inlet temperature of GT and compression ratio of AC_4 on total performance criteria.

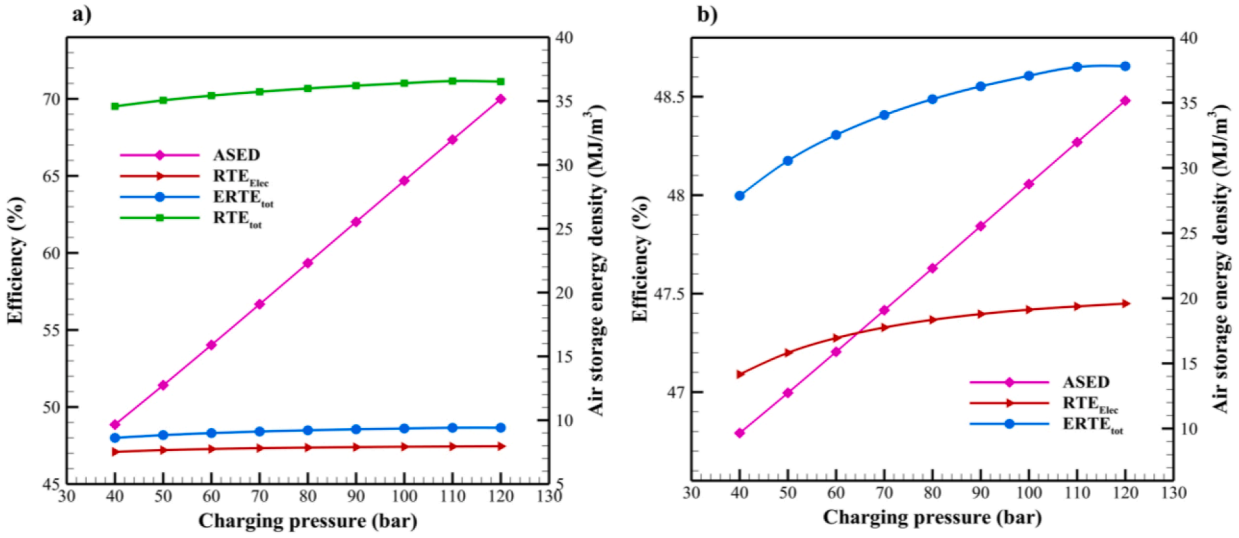

Fig. 9. The effect of CAES charging pressure level on the overall performance criteria of the system.

Table 11
The result of exergoeconomic analysis for different components of the system.

component	$c^f(\$/GJ)$	$c^p(\$/GJ)$	$f_k(\%)$	$r_k(\%)$	$\dot{C}^D(\$/hr)$	$\dot{Z}(\$/\mathrm{hr})$
Aftercooler	11.3	11.91	31.09	5.480	1.27	0.570
Air compressor 1	6.69	11.31	84.75	69.05	8.16	45.37
Air compressor 2	6.69	11.29	84.75	68.75	8.21	45.66
Air compressor 3	6.69	11.28	84.75	68.67	8.23	45.74
Air compressor 4	6.69	8.100	61.45	21.12	17.8	28.38
Air turbine	8.27	13.03	75.20	57.59	60.6	183.9
CAES tank	11.3	6.520	100.0	42.20	0.00	46.08
Combustion chamber	4.12	5.150	2.580	25.11	80.5	2.130
Condenser 1	2.53	4.300	7.650	70.06	28.3	2.340
Condenser 2	6.10	17.63	49.37	188.9	4.14	4.040
Cold oil tank	0.00	0.000	100.0	100.0	0.00	8.280
Evaporator 1	2.01	2.510	17.33	24.67	25.5	5.350
Evaporator 2	3.90	5.530	14.42	41.96	24.3	4.100
Expansion valve	2.01	0.000	48.72	100.0	0.53	0.510
Flue gas condensation 1	6.02	23.00	10.48	282.3	8.73	1.020
Flue gas condensation 2	6.02	28.22	34.51	368.9	9.31	4.900
Gasifier	2.62	4.120	8.010	57.15	137	11.94
Gas turbine	6.02	6.690	63.93	11.13	20.5	36.31
Heat exchanger 1	6.07	13.68	9.090	125.3	21.7	2.170
Heat exchanger 2	6.02	6.640	16.55	10.41	9.37	1.860
Heat exchanger 3	2.01	12.48	99.44	519.8	0.12	21.68
Hot oil tank	9.64	2.010	100.0	79.11	0.00	7.560
Hot water tank 1	11.8	6.070	100.0	48.51	0.00	3.067
Hot water tank 2	23.0	5.950	100.0	74.15	0.00	3.960
Intercooler 1	11.3	11.79	48.58	4.320	0.70	0.670
Intercooler 2	11.3	11.74	51.91	3.980	0.63	0.680
ORC turbine	6.10	18.74	88.64	206.9	19.3	150.3
Pump 1	6.69	1025	21.32	15,231	0.09	0.020
Pump 2	10.7	14.25	43.40	32.91	0.18	0.130
Pump 3	18.7	23.69	7.890	26.43	2.59	0.220
Recuperator 1	6.02	6.320	9.680	5.080	21.5	2.310
Recuperator 2	6.02	6.080	4.650	1.060	3.59	0.170
Regulation valve	6.52	8.630	0.260	32.23	83.03	0.210
Steam turbine	2.53	10.72	97.44	324.2	6.53	249.0
Water pump	6.69	9.220	33.87	37.87	0.13	0.070

Here $\dot{C}_{tot}$ represents the total expenses rate of the system in $(\$/hr)$ which is the sum of the cost rates of system components, exergy destruction, biomass feedstock, and emitted CO_2. The sum unit cost of products ($SUCP$) is expressed by Eq. (43). The sum of product cost rates to their exergy rates determines $SUCP$ as an overall thermoeconomic criteria. Another important parameter in thermoeconomic analyses which is extensively used for energy-related systems or power plants is the Levelized Cost of electricity ($LCOE$) that is calculated by the division of the total cost rate of the unit to the total generated power. This item also determines the minimum value of the product which is electricity in this case.

3.4. Economic analysis

Among various methods for economic investigations, the net present value (NPV) has been chosen to be used in this study. The profitability and the payback period of the proposed system are calculated through this method. Thus, the net cash flow at the end of each year is converted to the present value as follow [1]:

$$NPV_n = \sum_{n=0}^{N} Y(r+1)^{-n} \tag{45}$$

Here n, N, r respectively define the year, system lifespan, and the discount rate. Also Y denotes the cash flow at the end of each year. Meanwhile, it must be indicated that the payback period is the time that it takes for the NPV value to equal the total investment cost of the system.

3.5. Environmental analysis

Unfortunately, the environmental impacts of energy-related systems are neglected most of the time in different projects. Therefore some inefficient and hazardous technologies from environmental approaches are employed in different sectors [50]. In this regard, analyzing these systems from an environmental perspective is an imperative assessment that should be considered as well as thermodynamic and economic analyses [51]. GHG emissions and thermal pollutions are some of the conventional and destructive side effects of power plants. These pollutions are the cause of various phenomena like global warming, ozone layer depletion, ocean acidification, shrinkage of ice sheets and consequently rising the oceans water level. Regrettably, human beings are responsible for the majority of these disasters and there should be strong international regulations and commitments about these problems. The proposed configuration in this study not only covers the energy requirements of human societies economically but also introduces a negative carbon emission system that is fascinating and mandatory for saving the earth and its inhabitants from an impending disaster. In addition to all of the mentioned advantages, this system provides even more financial benefits by preventing from paying high CO_2 emission taxes. Eq. (46) demonstrates the rate of these financial savings [52]:

$$\dot{C}_{EnvSave} = 3.6 \times TAX_{CO_2} \cdot \dot{m}_{CO_2} \tag{46}$$

Where TAX_{CO_2} is the cost of producing CO_2 emission which is almost about 24 $/tonne in the United States and far higher values in Europe.

To have a comprehensive overview of environmental issues, life cycle assessment (LCA) which is a complementary methodology for analyzing the negative environmental effects of the products has been carried out particularly for CO_2 emission. It should be noted that a true LCA can generally be very demanding to do (including detailed calculation of environmental impacts of the system from the manufacturing process of one by one of the components, the plant's construction, its operation, and even its recycling or disposal), which is evidently out of

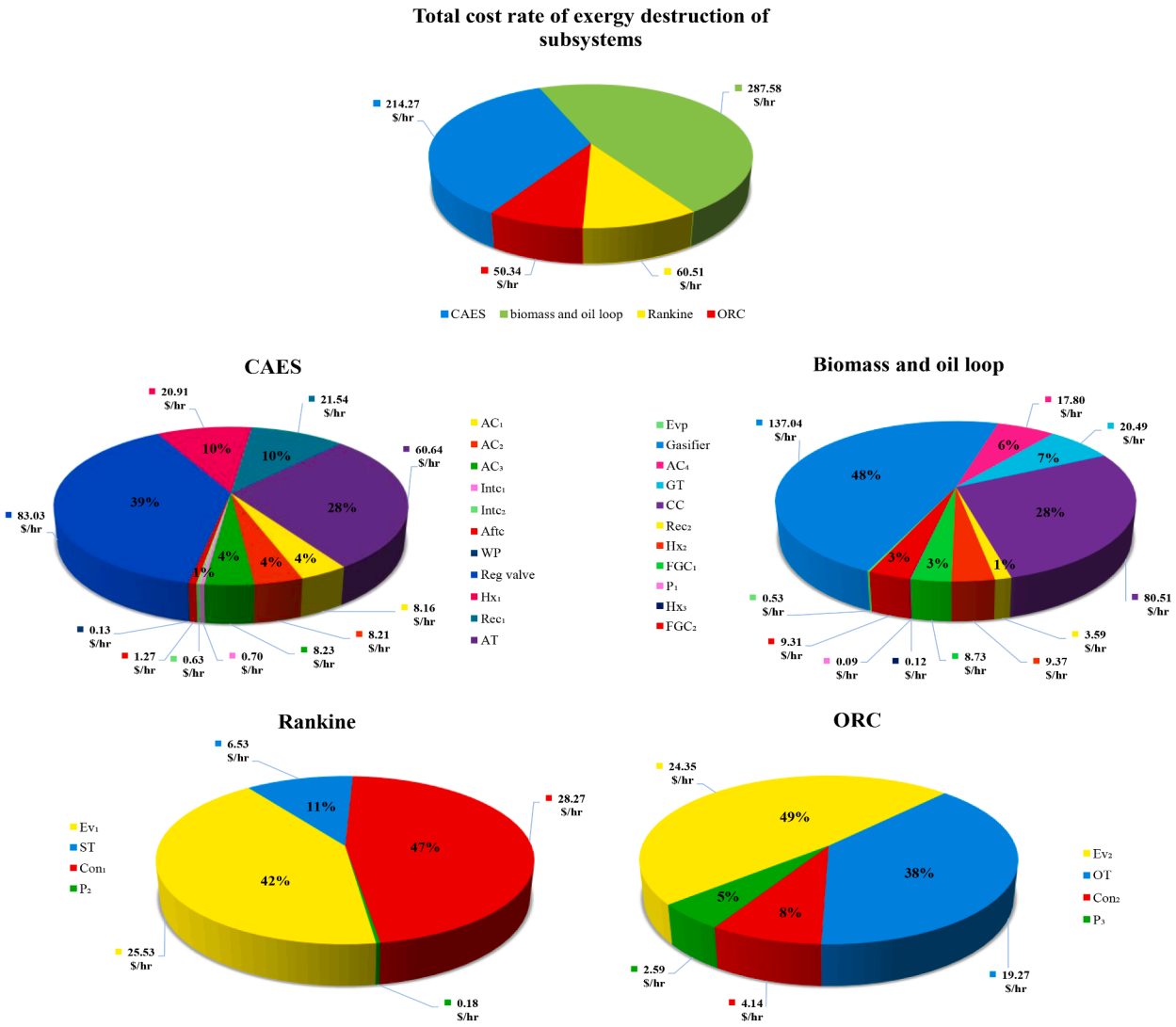

Fig. 10. The portion of exergy destruction cost rate for different subsystems and components.

the scope of this work. The LCA conducted here is a special type of environmental analysis based on two stages: well-to-pump (WtP) which considers the extraction and transferring procedure of the resources to the plant, and pump-to-production (PtP) as the processes taking place inside the plant to produce the products. The required information for WtP processes is obtained for the U.S in 2020 from GREET software [53].

3.6. Performance criteria

Due to the various operating times for different units of the system, the conventional methods for calculation of the thermodynamic efficiencies cannot be applied to such systems. In this regard, energetic and exergetic round-trip efficiencies are employed as the following equations to provide a general description of the system performance [25]:

$$RTE_{tot} = \frac{\left[24\cdot\dot{W}_{GT} + t_{dch}\left(\dot{W}_{AT} + \dot{W}_{ST} + \dot{W}_{OT} + \dot{Q}_{DHW}\right)\right]}{\left[24\left(\dot{W}_{AC_4} + \dot{Q}_{biomass}\right) + t_{ch}\left(\sum_{i=1}^{3}\dot{W}_{AC_i} + \dot{W}_{WP}\right) + t_{dch}\left(\sum_{i=2}^{3}\dot{W}_{P_i}\right) + \dot{W}_{P_1}(24 - t_{dch})\right]} \quad (47)$$

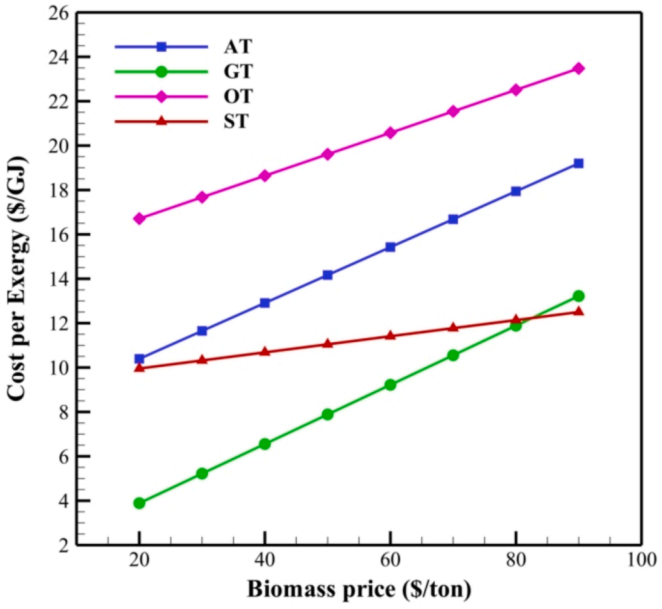

Fig. 11. The impact of biomass price on cost per exergy of different turbines of the proposed system.

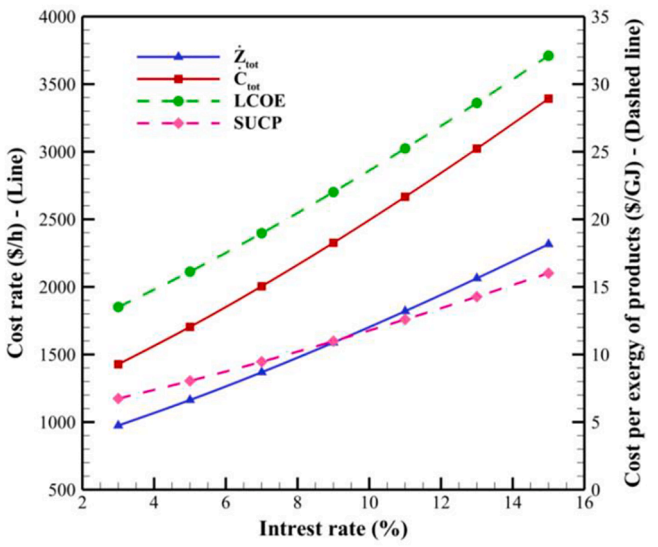

Fig. 12. The effect of interest rate alteration on overall thermoeconomic performance criteria.

$$ERTE_{tot} = \frac{\left[24\cdot\dot{W}_{GT} + t_{dch}\left(\dot{W}_{AT} + \dot{W}_{ST} + \dot{W}_{OT} + \dot{E}x_{Q_{DHW}}\right)\right]}{\left[24\left(\dot{W}_{AC_4} + \dot{E}x_{biomass}\right) + t_{ch}\left(\sum_{i=1}^{3}\dot{W}_{AC_i} + \dot{W}_{WP}\right) + t_{dch}\left(\sum_{i=2}^{3}\dot{W}_{P_i}\right) + \dot{W}_{P_1}(24 - t_{dch})\right]} \tag{48}$$

$$RTE_{Elec} = \frac{\left[24\cdot\dot{W}_{GT} + t_{dch}\left(\dot{W}_{AT} + \dot{W}_{ST} + \dot{W}_{OT}\right)\right]}{\left[24\left(\dot{W}_{AC_4} + \dot{Q}_{biomass}\right) + t_{ch}\left(\sum_{i=1}^{3}\dot{W}_{AC_i} + \dot{W}_{WP}\right) + t_{dch}\left(\sum_{i=2}^{3}\dot{W}_{P_i}\right) + \dot{W}_{P_1}(24 - t_{dch})\right]} \tag{49}$$

$$RTE_{\text{stand - alone biomass plant}} = \frac{\dot{W}_{GT}}{\dot{Q}_{biomass} + \dot{W}_{AC_4}},\ \dot{Q}_{biomass} = \dot{m}_{biomass}\cdot HHV_{biomass} \tag{50}$$

In addition to the energetic and exergetic efficiencies, energy density is another critical parameter in systems with energy storage units. Therefore, the air storage energy density (ASED) factor is defined as follow [1]:

$$ASED = \frac{3.6 \times t_{dch} \times \dot{W}_{AT}}{V_{CAES}} \tag{51}$$

This factor is the ratio between the total generated power in the discharge period and the total storage volume capacity which is also an appropriate tool for comparison between different energy storage technologies.

4. Validation

As aforementioned in previous sections, the proposed configuration of this system is studied for the first time in the literature. In this regard, for verification of the simulation method, different units of this system are validated with authentic publication and experimental results. Table 7 shows the mole percent of different compositions in the gasifier. The mole percent of the products are compared with the experimental results of Alauddin [54]. The simulation results of the other units of this system are validated with different publications. With less than 10%, the calculated errors in Table 8 demonstrate good agreement between the obtained results and the related investigations.

5. Results and discussion

In this section, the results of the analyses are presented and discussed as well. Comprehensive diagrams and tables are dedicated to each part

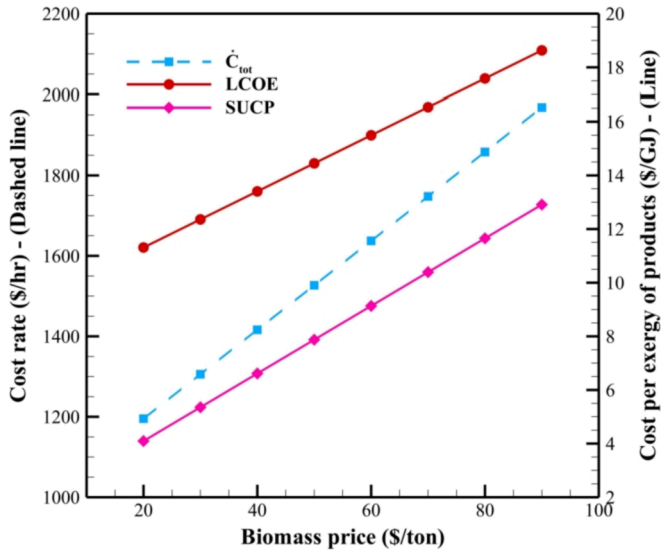

Fig. 13. The effect of biomass price alteration on overall thermoeconomic performance criteria.

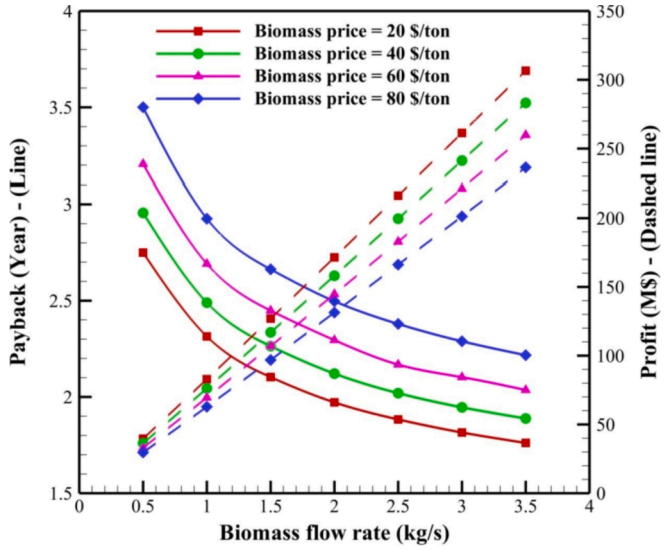

Fig. 14. The simultaneous effect of biomass price and flow rate alteration on overall economic criteria.

to provide better visuals about the results. Also, parametric analysis is performed to examine the impact of critical parameters on the overall performance of the system. It is worth mentioning that the parametric analysis of each category (thermodynamic, economic, thermoeconomic, and environmental) are performed and illustrated in their own segment.

5.1. Thermodynamic analysis

Thermodynamic analyses from both energetic and exergetic viewpoints are accomplished for the proposed cycle. Critical properties of each stream are tabulated by Table 9 which provides a better comprehension of the system operation procedure. Also, the significant results of the analyses are listed in Table 10.

Based on the proposed system configuration in Fig. 1, 10.76 MW power is consumed by CAES compressors to pressurize the ambient air until 90 bar. The compressed air is stored during 8 h of off-peak time in the CAES tank and 11 MW heat of compression is captured by Inter/Aftercoolers. Then during 4 h of peak demand period, the stored air is

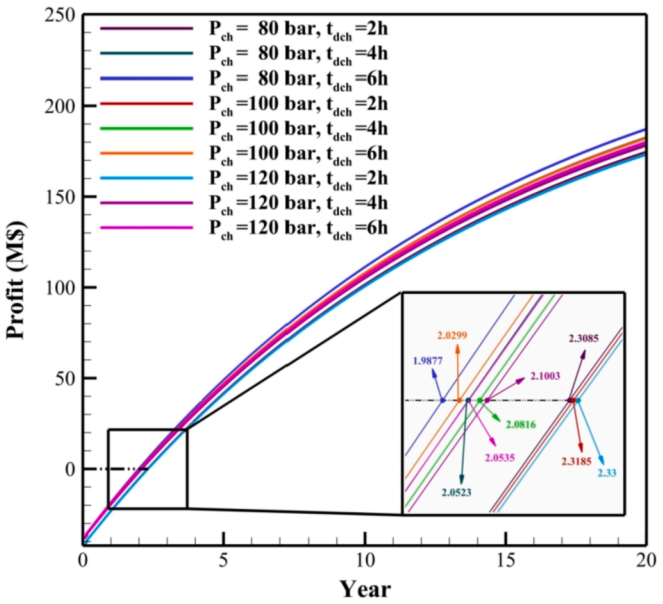

Fig. 15. The effect of different CAES charging pressures in various discharge periods on the total profit and payback period.

discharged from the tank. Primarily, the pressure is regulated in the Reg valve to the level of 30 bar and then the proposed stream is preheated in two stages of Hx_1 and Rec_1. After receiving 15.23 MW heat, the pressurized air stream expands in the AT to the ambient pressure and generates 14.26 MW electricity. During the charging mode of the CAES unit, 486 m^3 pressurized hot water is produced and stored in the HWT_1 for further utilization in on-peak times. On the other hand, the stand-alone biomass power plant is under operation for 24 h. The wood chips as the biomass feedstock enter the gasifier unit besides a specific amount of air. After passing four stages of drying, pyrolysis, combustion, and reduction in an oxygen-starved condition the final product is a gaseous mixture called syngas and the residual by-product is unreacted carbon so-called char. 9.82 MW power is employed to compress the ambient air in AC_4. Also, 8.1 MW heat is exchanged between the outlet streams of the GT and AC_4. The syngas is combusted with excess air and the produced flue gas reaches 1400 K before entering the GT. The superheated flue gas stream expands to the ambient pressure in GT and generates 23.55 MW of electrical power. During 20 h of mid and off-peak periods, the thermal energy of flue gas (13.5 MW) is stored in the thermal oil (Therminol VP1) which showed great characteristics in thermal storage duty among the other substances. The residual heat of the flue gas during the 20 h of the BC operation is captured in FGC_1. FGC units are designed to accomplish two important tasks simultaneously. Utilizing the latent heat of vapor and eliminating H_2O from the flue gas streams to prevent possible damages like corrosion that can be caused by acidic solutions (H_2O + (CO_2 or NOx/SOx)→acidic solutions)[53]. With this in mind, 5.13 MW heat is recovered in FGC_1. In 4 h of peak demand period, the heat of the flue gas stream (state 41) is transferred to the compressed air via Hx_1. Then the residual heat of the flue gas is respectively exchanged in Ev_2 and FGC_2 with the same procedure that was explained previously. The stored hot thermal oil during 20 h completes the oil loop flowing into the Ev_1 (45.52 MW), Ev_2, and Hx_3 (7.54 MW) as the heat source of RC and ORC and also producing DHW in 4 h of on-peak. The pressurized hot water stream (state 22) is another heat source for the ORC unit and with the overall 26.88 MW heat in Ev_2, the ORC unit operates as well as the RC unit during the on-peak period. The saturated liquid ammonia (state 66) enters the Ev_2 and after capturing 26.88 MW, the superheated gas expands in OT to the saturated vapor state and then generates 3.73 MW electricity. Saturated vapor turns into the saturated liquid state via Con_2 (23.34 MW) then is pressurized to a desired pressure level by P_3

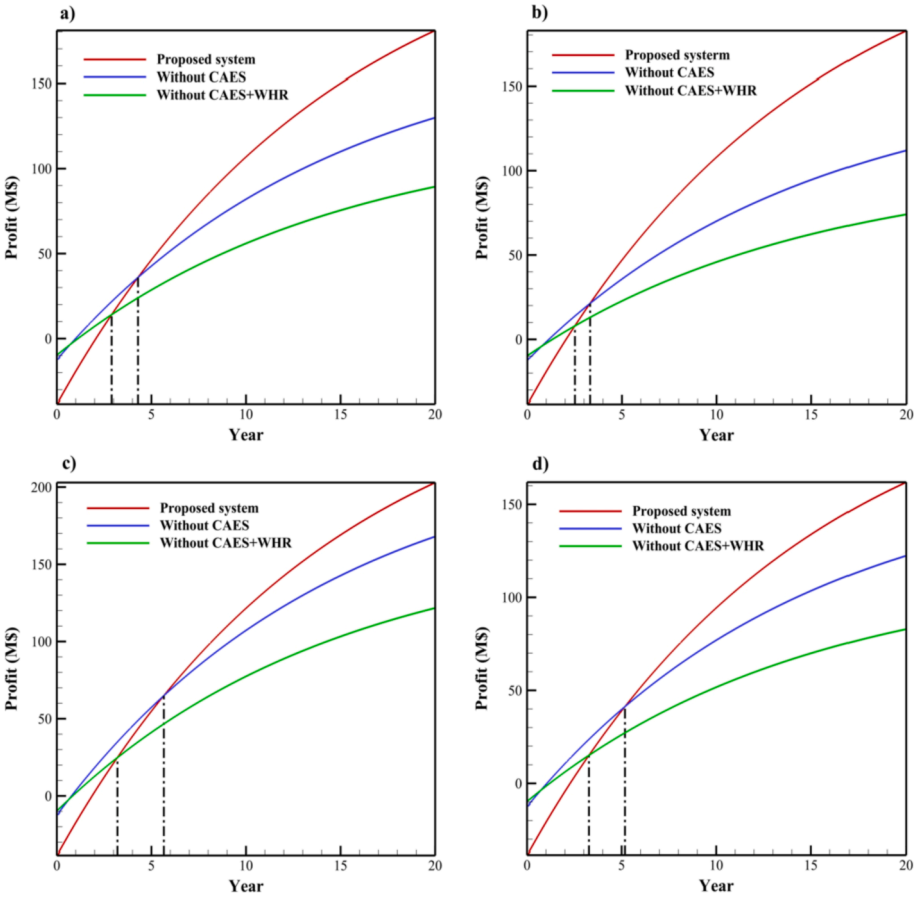

Fig. 16. Comparison of different configurations of the proposed system with different on-peak and off-peak electricity prices.

(195.8 kW). The same operations take place for RC and eventually the significant results are illustrated in Table 9 as well. With 348.34 MWh net produced power and 615.67 MWh total exergy destruction for the entire system, the proposed configuration in this study demonstrates outstanding thermodynamic performance by ~ 71% total RTE and 49% ERTE. Also, this cogeneration system shows ~ 67% and 11.5% total and electrical RTE improvements in comparison to the stand-alone biomass plants without the utilization of CAES and WHR systems. For better visualization of the discussed topic in this section, Fig. 2 is presented as well. This plot shows the share of power generation and consumption for each unit and its components.

To avoid laboring the discussed topics for the exergy approach, Fig. 3 represents the exergy destruction value of each subsystem and component. As it's shown in Fig. 3, the major portion of exergy destruction in each unit is dedicated to evaporators, condensers, pressure regulation valve, gasifier, and combustion chamber.

Through the thermodynamic simulation of the proposed system in this study, a lot of heat exchangers in different kinds are considered and modeled. The pinch point temperature difference is one of the important characteristics of each heat exchanger which are assumed as listed in

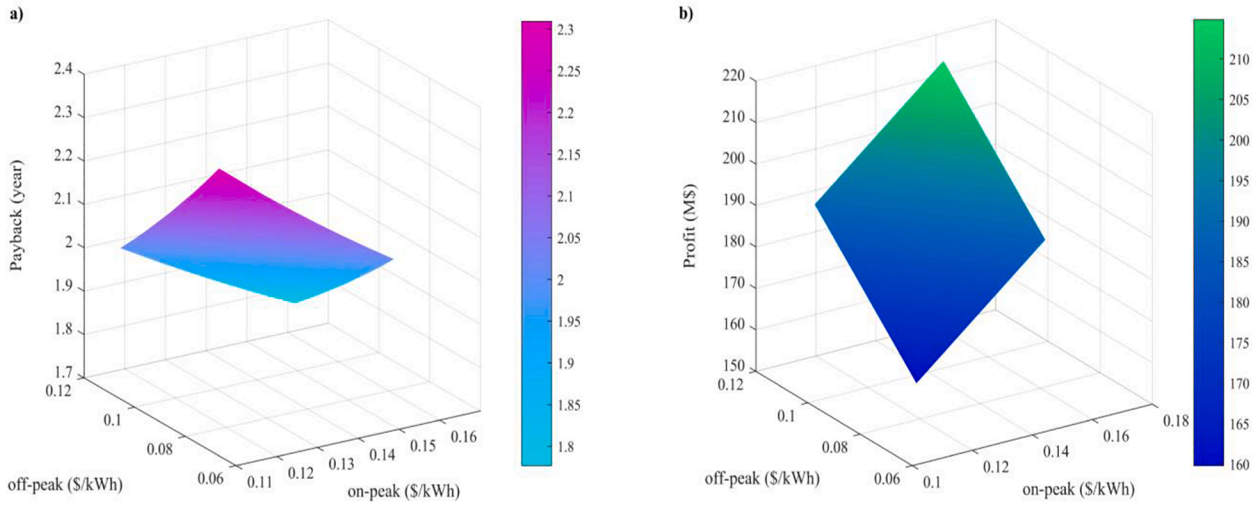

Fig. 17. The impact of on-peak and off-peak electricity price alteration on a) payback period, b) total profit.

Table 12
Emitted pollutants during the well-to-pump processes of supplying biomass feedstock.

Pollutants	Value (tonne/year)
CO_2	2441.52
VOC	0.7138
CO	5.3548
NOx	6.87
PM10	0.4554
PM2.5	0.3579
Sox	0.1415
CH_4	2.976
N_2O	0.0291
BC	0.2452
POC	0.0747
GHG-100	2548.602

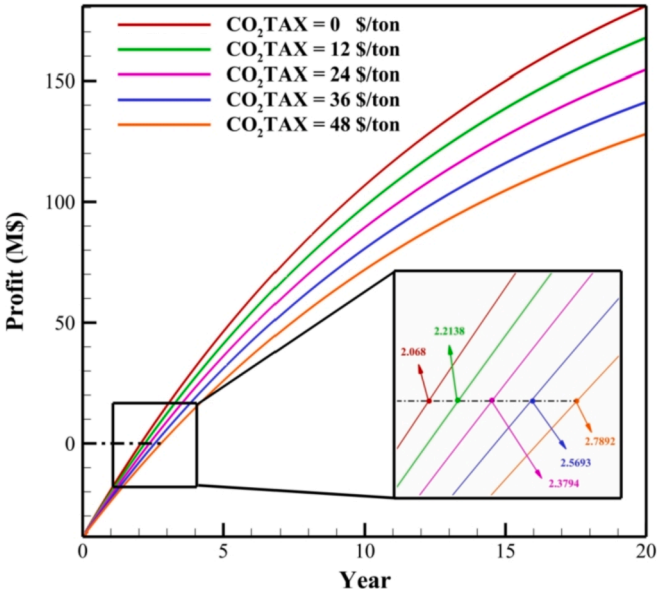

Fig. 18. The effect of CO_2 tax level on total profit and payback period of the proposed biomass-based CHP + CAES system.

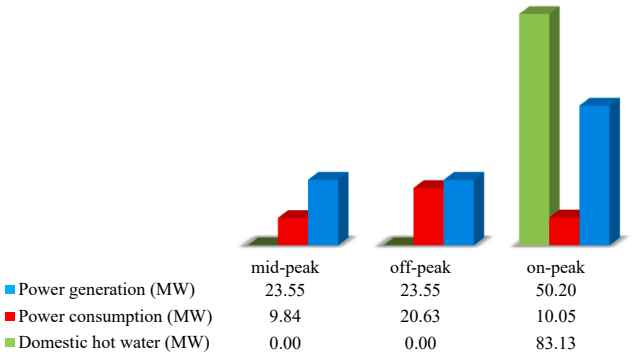

Fig. 19. The share of power generation/consumption and DHW production in each period for the proposed biomass-based CHP + CAES system.

Table 1. Composite curves are viable plots that demonstrate the hot and cold streams with their specific heat duties and also are great tools to control and avoid pinch crossing issues. Fig. 4 illustrates the composite curve of different heat exchangers and affirms that there is no crossing problem at pinch points.

The gasifier is the heart of each biomass power plant and the parametric analysis on this part is valuable and essential. Therefore Fig. 5 represents the effect of gasification temperature on different parameters. In part (a) of this figure, the relationship between the gasification temperature, LHV of syngas, and syngas composition is assessed. As it's shown, the LHV will decrease by the increment of gasification temperature. This is based on the fact that by increasing the gasification temperature the molar fraction of CH_4 and H_2 as flammable components is decreasing and the CO is almost constant. Also, the composition of H_2O and N_2 are increasing while CO_2 experiences a slight decrement. Altogether to see the impact of gasification temperature on the overall efficiencies part (b) of Fig. 5 is presented. Based upon this figure, after the design gasification temperature (1023 K), the total and electrical RTE and ERTE are almost constant which means further increment of gasification temperature is ineffective and also may increase the risk of production of some other harmful pollutions (like NOx) based on the rise of nitrogen level. Although increasing the syngas temperature causes more power production, the figure shows that fuel consumption and CO_2 emission level increase and this leads to worse environmental conditions and constant RTE values.

The following figure is about the effect of biomass flow rate alteration on power generation/consumption of different components. Fig. 6 demonstrates the fact that the increment of biomass feedstock will drastically affect GT power production. The produced power of other turbines is enhanced too based on the increment of total input energy of the system. The syngas and CO_2 production rate will increase too.

The effect of unreacted carbon (char) percentage on the system's overall performances is analyzed and displayed in Fig. 7. Due to this plot, the overall efficiencies will reduce by the increment of char level. Consequently, the required amount of air and biomass feedstock is flourished to compensate the wasted unreacted carbon.

The following figure is dedicated to the BC unit and includes four related plots which show the relationship between the GT inlet temperature, the compression ratio of AC_4, and different critical parameters. Part (a) of Fig. 8 shows that the increment of the AC_4 compression ratio requires a higher amount of syngas which leads to higher fuel–air (FA) ratios. Also, for higher inlet temperatures of GT more FA ratios are attained. More fuel means more energy production and consequently more fuel consumption. Therefore the total RTE values will generally increase and this improvement is even more remarkable for lower GT inlet temperatures. Part (b) of Fig. 8 illustrates the influence of the mentioned parameters on total RTE. Also, Part (c) of Fig. 8 displays that higher inlet temperature for the GT is better for electricity production capacity only at higher compression ratios. The ERTE values show almost the same results as the electrical RTE and this is tabulated in part (d) of Fig. 8.

Fig. 9 is dedicated to the impact of CAES charging pressure on the overall performance of this system. The ASED value is constantly increased by the increment of charging pressure. Because compressing the air leads to higher power production in discharge mode and also a lower volume of the storage tank. Also, the RTE and ERTE values are almost constant with the variation of charging pressure but based on the further details in part (b), it can be concluded that there is a slight improvement after 90 bar of charging pressure.

5.2. Thermoeconomic analysis

In this section, the thermoeconomic results are presented by various tables and figures. The cost per exergy of the ambient air and water is considered to be 0 $/GJ while the biomass feedstock has the value of 2.621 $/GJ. After thermoeconomic calculations and solving the cost balance equations for each component of the system, the cost per exergy unit of each stream and also cost rates of different streams and components are obtained. Cost rates and cost per exergy of different streams are tabulated in Table 9. Also, Table 11 represents the significant results of Exergoeconomic analysis for different components of the system. The relative cost difference, exergoeconomic factor, cost rate of exergy destructions, and cost per exergy of fuel and product for each component

are listed in Table 11.

The share of the cost rate of exergy destruction for different subsystems and their components is illustrated by the pie chart in Fig. 10. Due to the obtained results from this figure, the greatest portion of the cost rate of exergy destruction values are respectively dedicated to biomass plant and thermal oil loop, CAES, RC, and ORC. Generally, it can be pointed out that the components with greater exergy destruction values have the largest portion of the cost rate of exergy destructions too.

The effect of biomass price on the cost per exergy of the turbines is figured out by Fig. 11. An increment of biomass price from 20 $/tonne to 90 $/tonne results in enhancement of cost per exergy of products. Based on the results, it can be concluded that the OT has the highest cost per exergy value among other turbines. Also, the alteration of biomass price has the lowest effect on ST in comparison to the other turbines.

In the following figures, the effect of biomass price and interest rate on the overall thermoeconomic performance criteria are evaluated. Fig. 12 elaborates the fact that by interest rate growth, the total cost and expenses rates will rise. Also, it can be pointed out that the increment of interest rate has a little bit more impact on *LCOE* and total expenses rate. On the other hand, according to the evidence that emerges from Fig. 13, the *SUCP* and *LCOE* values experience almost the same increment trend based on the variation of biomass price. Total expenses rate is also increased by about 800 $/hr for 70 unit increment in biomass price in $/tonne. As a result, it is worth mentioning that a 5% increment of interest rate has almost the same effect on *LCOE* as a 70 $/tonne increment of biomass price does.

5.3. Economic analysis

The final section of results and discussion is assigned to the economic aspects of the proposed system which provides a great oversight on the profitability of this project. The effect of biomass price and flow rate on profit and payback values is the topic of the first diagram which is illustrated in Fig. 14. In reference to this figure, it can be concluded that for lower biomass prices the profits are higher and the payback period is shorter. On the other side, the effect of biomass flow rate on profit and payback is steeper until the amount of 1.5 kg/s. This means lower payback periods and higher profits are achievable in higher biomass flow rates and it determines the fact that the proposed system is more profitable for grid-scale applications.

One of the important parameters in the parametric study of such systems is charge/discharge pressures and periods. The influence of different charging pressures with various discharging times is the subject of Fig. 15. Comparison between the best and the worst scenario in this section demonstrates only 3 months difference between these two conditions. Generally, the best possible condition for this system occurs in lower charging pressures and longer discharge periods. More details are available in Fig. 15.

Another crucial parameter that directly affects the economic aspect of such a CHP plant is the price of electricity. This item is scrutinized through two different figures with various scenarios to provide a precious comparison for the readers. Fig. 16 determines the effect of on-peak and off-peak electricity prices in four different scenarios for different configurations of the proposed system. In part (a) of Fig. 16, the electricity prices are set as the design condition values which are mentioned in Table 1. Part (b) shows the case in which the on-peak electricity price is 20% more than the design value and the off-peak price is 20% lower than 0.09756 $/kWh. In part (c), the on-peak and off-peak electricity prices are both equal to the case study value of on-peak electricity price (0.12801 $/kWh). And the last part (part (d)) is as same as part (c) but both prices are equal to 0.09756 $/kWh which is the price of off-peak electricity in design condition. Three different configurations of the proposed system are the main state, the system without CAES unit, and the system without CAES and WHR units. This comparison aims to demonstrate the significance of combined technologies with a stand-alone biomass plant. Due to the figures, although the stand-alone state shows lower payback periods but when it comes to profitability the proposed system overcomes the basic approaches. Part (a) elaborates that the attained profit of the proposed system passes the stand-alone and without CAES configurations in the third and the fourth year of the system lifespan. With more than 90 M$ at the end of the plant lifespan, the proposed system demonstrates great economic superiorities rather than the stand-alone condition. The best scenario among these four conditions is dedicated to part (b) in which the on-peak prices are high and the off-peak prices are low. Further details are visualized through Fig. 16.

Also, Fig. 17 shows a 3D plot about the effect of on-peak and off-peak electricity prices on the payback and profit criteria. As shown, the payback and profit values are respectively decreased and increased with electricity price increment either for on-peak or off-peak periods.

5.4. Environmental analysis

In this section, the results of environmental analyses are presented and discussed. The proposed plant demands 71996.67 tonnes of wood chips per year. Based on the analyses carried out by GREET software, the overall emitted pollutants for the WtP processes (cutting the trees, transportation of resources with heavy trucks, etc.) are listed in Table 12.

The emitted CO_2 has the highest value in WtP processes. Likewise, the major emission of the plant while operating is CO_2. Therefore, the LCA is conducted for CO_2 emission. 50 wt% of the feedstock composition is made of carbon which means 1 kg of feedstock is able to absorb 1.83 kg of CO_2. Thus, the feedstock of the introduced configuration in this study can absorb 131753.9 tonnes of the existing CO_2 in the atmosphere while it only emits 103566.12 tonnes of CO_2 per year during PtP processes. All in all, with 25746.26 tonnes of excess captured CO_2 per year, the introduced system demonstrates negative-carbon characteristics. Also, the unreacted carbon disposed of the gasifier can be utilized either in different industries or as soil carbon which is absolutely essential for agricultural purposes.

Despite being environmentally friendly, the proposed configuration benefits from being a negative carbon system. In terms of considering the high amount of CO_2 emission taxes, the introduced system is counted as one of the decisive choices in energy-related sectors. Fig. 18 displays the profit and payback period for five different CO_2 tax values. 7 months reduction of payback period and around 50 M$ profit are two of the outstanding achievements of this system with considering 0 and 48 $/tonne CO_2 taxes.

Ultimately, Fig. 19 describes the generated/consumed electricity and hot water in each period of the day. This figure clarifies that the produced energy in mid and off-peak periods is remarkably lower than the on-peak time and this eliminates the mismatches between the power production rate and the grid demand. Also, the net produced power in off-peak is lower than other times because a significant amount of energy supplied by the biomass plant is stored via the CAES system. Generally, this system benefits from avoiding CO_2 tax payment and producing more energy in peak periods in which the energy price is higher than the other times of the day.

6. Conclusion

In the path of saving the earth from an impending disaster, a lot of research is conducted on the clean methods of producing human society demands. Energy, especially in two forms of electricity and heat is the most essential and intrinsic part of life in this era. The proposed multi-generating hybrid biomass-driven CHP plant with the utilization of the CAES system of this study proposes a lot of thermoeconomic and environmental advantages in comparison to the older concepts. Multi-generating heat and power taking advantage of the net negative emission feature of the biomass source makes the system a quite valuable

design from an environmental impact perspective. The basic concept of the biomass power plant has been optimized with different cutting-edge technologies to provide better overall performance and consequently significant economic achievements. The addition of a grid-scale energy storage system like CAES improves drastically the economic potentials of this system, besides offering flexibility, load-leveling/shifting, and peak shaving to the electricity grid.

The most significant conclusions of this research are summarized as follow:

- With around 71% total RTE and 47.4% electrical RTE, the proposed system shows ~ 67% and 11.5% improvement of RTE in comparison to the stand-alone biomass power plant.
- With 40 MW net generated power in on-peak, 14 MW in mid-peak, and around 3 MW during off-peak periods, the proposed system demonstrates great potentials for power shifting purposes. Also, 6651.4 m^3 DHW is generated each day through the operation of the system.
- The FGC units prevent the corrosion of structures by condensation of H_2O components from the flue gas stream. Also, 10.56 MW heat is recovered in FGC units from the flue gas stream. Most of this energy is captured by the latent heat of the existing vapor in the flue gas.
- After the third year of the system operation, the proposed configuration overtakes the stand-alone concept in terms of total profit. The financial difference between these two configurations is ~90 M$ profit at the end of their lifespans. Only 2 years is the payback period of the proposed biomass-based CHP + CAES system.
- Considering 48 $/tonne carbon tax results in 50 M$ reductions of total profit at the end of the 20th year. This will of course turn to higher values where higher emission tax rates are applied.
- Based on the attained results from the life cycle assessment, it has been concluded that the net captured CO_2 by the proposed system of this study was 25764.26 tonnes per year which showcases the carbon-negative feature of the introduced biomass-based configuration.
- The LCOE is ~13.51 $/GJ (or 0.05 $/kWh) while the average electricity price in the United States is about 0.1 $/kWh. This means the proposed system generates electricity with lower costs rather than the market price for the case study of the United States.

CRediT authorship contribution statement

Fatemeh Lashgari: Conceptualization, Methodology, Investigation, Software, Visualization, Project administration. **Seyed Mostafa Babaei:** Conceptualization, Methodology, Investigation, Software, Visualization, Validation, Formal analysis. **Mona Zamani Pedram:** Conceptualization, Supervision. **Ahmad Arabkoohsar:** Supervision.

Declaration of Competing Interest

The authors declare that they have no known competing financial interests or personal relationships that could have appeared to influence the work reported in this paper.

References

[1] Nabat MH, Zeynalian M, Razmi AR, Arabkoohsar A, Soltani M. Energy, exergy, and economic analyses of an innovative energy storage system; liquid air energy storage (LAES) combined with high-temperature thermal energy storage (HTES). Energy Convers Manag 2020;226:113486. https://doi.org/10.1016/j.enconman.2020.113486.

[2] Sohani A, Sayyaadi H, Mohammadhosseini N. Comparative study of the conventional types of heat and mass exchangers to achieve the best design of dew point evaporative coolers at diverse climatic conditions. Energy Convers Manag 2018;158:327–45. https://doi.org/10.1016/j.enconman.2017.12.042.

[3] Babaei SM, Razmi AR, Soltani M, Nathwani J. Quantifying the effect of nanoparticles addition to a hybrid absorption/recompression refrigeration cycle. J Clean Prod 2020;260:121084. https://doi.org/10.1016/j.jclepro.2020.121084.

[4] Razmi AR, Soltani M, Ardehali A, Gharali K, Dusseault MB, Nathwani J. Design, thermodynamic, and wind assessments of a compressed air energy storage (CAES) integrated with two adjacent wind farms: A case study at Abhar and Kahak sites. Iran. Energy 2021;221:119902. https://doi.org/10.1016/j.energy.2021.119902.

[5] Razmi AR, Heydari Afshar H, Pourahmadiyan A, Torabi M. Investigation of a combined heat and power (CHP) system based on biomass and compressed air energy storage (CAES). Sustain Energy Technol Assessments 2021;46:101253. https://doi.org/10.1016/j.seta.2021.101253.

[6] Zhang X, Li H, Liu L, Bai C, Wang S, Song Q, et al. Exergetic and exergoeconomic assessment of a novel CHP system integrating biomass partial gasification with ground source heat pump. Energy Convers Manag 2018;156:666–79. https://doi.org/10.1016/j.enconman.2017.11.075.

[7] Habibollahzade A, Gholamian E, Houshfar E, Behzadi A. Multi-objective optimization of biomass-based solid oxide fuel cell integrated with Stirling engine and electrolyzer. Energy Convers Manag 2018;171:1116–33. https://doi.org/10.1016/j.enconman.2018.06.061.

[8] Wu C-Z, Yin X-l, Ma L-L, Zhou Z-Q, Chen H-P. Operational characteristics of a 1.2-MW biomass gasification and power generation plant. Biotechnol Adv 2009;27(5):588–92. https://doi.org/10.1016/j.biotechadv.2009.04.020.

[9] Khalid F, Dincer I, Rosen MA. Energy and exergy analyses of a solar-biomass integrated cycle for multigeneration. Sol Energy 2015;112:290–9. https://doi.org/10.1016/j.solener.2014.11.027.

[10] Razmi AR, Janbaz M. Exergoeconomic assessment with reliability consideration of a green cogeneration system based on compressed air energy storage (CAES). Energy Convers Manag 2020;204:112320. https://doi.org/10.1016/j.enconman.2019.112320.

[11] Assareh E, Alirahmi SM, Ahmadi P. A Sustainable model for the integration of solar and geothermal energy boosted with thermoelectric generators (TEGs) for electricity, cooling and desalination purpose. Geothermics 2021;92:102042. https://doi.org/10.1016/j.geothermics.2021.102042.

[12] Dong L, Liu H, Riffat S. Development of small-scale and micro-scale biomass-fuelled CHP systems – A literature review. Appl Therm Eng 2009;29(11-12):2119–26. https://doi.org/10.1016/j.applthermaleng.2008.12.004.

[13] Gholamian E, Mahmoudi SMS, Zare V. Proposal, exergy analysis and optimization of a new biomass-based cogeneration system. Appl Therm Eng 2016;93:223–35. https://doi.org/10.1016/j.applthermaleng.2015.09.095.

[14] Ahmadi P, Dincer I, Rosen MA. Development and assessment of an integrated biomass-based multi-generation energy system. Energy 2013;56:155–66. https://doi.org/10.1016/j.energy.2013.04.024.

[15] Razmi A, Soltani M, Aghanaja C, Torabi M. Thermodynamic and economic investigation of a novel integration of the absorption-recompression refrigeration system with compressed air energy storage (CAES). Energy Convers Manag 2019;187:262–73. https://doi.org/10.1016/j.enconman.2019.03.010.

[16] Razmi A, Zeynalian M, Hajialirezaei MH, Razmi AR, Torabi M. Carbon Dioxide Capture from Compressed Air Energy Storage System. Appl. Therm. Eng. 2020;178:115593. https://doi.org/10.1016/j.applthermaleng.2020.115593.

[17] Mason JE, Archer CL. Baseload electricity from wind via compressed air energy storage (CAES). Renew Sustain Energy Rev 2012;16(2):1099–109. https://doi.org/10.1016/j.rser.2011.11.009.

[18] Razmi A, Soltani M, Torabi M. Investigation of an efficient and environmentally-friendly CCHP system based on CAES, ORC and compression-absorption refrigeration cycle: Energy and exergy analysis. Energy Convers Manag 2019;195:1199–211. https://doi.org/10.1016/j.enconman.2019.05.065.

[19] Razmi A, Soltani M, Tayefeh M, Torabi M, Dusseault MB. Thermodynamic analysis of compressed air energy storage (CAES) hybridized with a multi-effect desalination (MED) system. Energy Convers Manag 2019;199:112047. https://doi.org/10.1016/j.enconman.2019.112047.

[20] Wang X, Yang C, Huang M, Ma X. Multi-objective optimization of a gas turbine-based CCHP combined with solar and compressed air energy storage system. Energy Convers Manag 2018;164:93–101. https://doi.org/10.1016/j.enconman.2018.02.081.

[21] Roushenas R, Razmi AR, Soltani M, Torabi M, Dusseault MB, Nathwani J. Thermo-environmental analysis of a novel cogeneration system based on solid oxide fuel cell (SOFC) and compressed air energy storage (CAES) coupled with turbocharger. Appl Therm Eng 2020;181:115978. https://doi.org/10.1016/j.applthermaleng.2020.115978.

[22] Shahverdian MH, Sohani A, Sayyaadi H. Water-energy nexus performance investigation of water flow cooling as a clean way to enhance the productivity of solar photovoltaic modules. J Clean Prod 2021;312:127641. https://doi.org/10.1016/j.jclepro.2021.127641.

[23] Razmi A, Soltani M, M. Kashkooli F, Garousi Farshi L. Energy and exergy analysis of an environmentally-friendly hybrid absorption/recompression refrigeration system. Energy Convers Manag 2018;164:59–69. https://doi.org/10.1016/j.enconman.2018.02.084.

[24] Babaei SM, Nabat MH, Lashgari F, Pedram MZ, Arabkoohsar A. Thermodynamic analysis and optimization of an innovative hybrid multi-generating liquid air energy storage system. J Energy Storage 2021;43:103262. https://doi.org/10.1016/j.est.2021.103262.

[25] Nabat MH, Soltani M, Razmi AR, Nathwani J, Dusseault MB. Investigation of a green energy storage system based on liquid air energy storage (LAES) and high-temperature concentrated solar power (CSP): Energy, exergy, economic, and environmental (4E) assessments, along with a case study for San Diego. US. Sustain Cities Soc 2021;75:103305. https://doi.org/10.1016/j.scs.2021.103305.

[26] McKendry P. Energy production from biomass (part 1): overview of biomass. Bioresour Technol 2002;83(1):37–46. https://doi.org/10.1016/S0960-8524(01)00118-3.
[27] Zainal ZA, Ali R, Lean CH, Seetharamu KN. Prediction of performance of a downdraft gasifier using equilibrium modeling for different biomass materials. Energy Convers Manag 2001;42(12):1499–515. https://doi.org/10.1016/S0196-8904(00)00078-9.
[28] Soltani M, Nabat MH, Razmi AR, Dusseault MB, Nathwani J. A comparative study between ORC and Kalina based waste heat recovery cycles applied to a green compressed air energy storage (CAES) system. Energy Convers Manag 2020;222:113203. https://doi.org/10.1016/j.enconman.2020.113203.
[29] Guo H, Xu Y, Chen H, Zhou X. Thermodynamic characteristics of a novel supercritical compressed air energy storage system. Energy Convers Manag 2016;115:167–77. https://doi.org/10.1016/j.enconman.2016.01.051.
[30] Alirahmi SM, Bashiri Mousavi S, Razmi AR, Ahmadi P. A comprehensive techno-economic analysis and multi-criteria optimization of a compressed air energy storage (CAES) hybridized with solar and desalination units. Energy Convers Manag 2021;236:114053. https://doi.org/10.1016/j.enconman.2021.114053.
[31] Soltani S, Mahmoudi SMS, Yari M, Rosen MA. Thermodynamic analyses of an externally fired gas turbine combined cycle integrated with a biomass gasification plant. Energy Convers Manag 2013;70:107–15. https://doi.org/10.1016/j.enconman.2013.03.002.
[32] Samadi SH, Ghobadian B, Nosrati M. Prediction and estimation of biomass energy from agricultural residues using air gasification technology in Iran. Renew Energy 2020;149:1077–91. https://doi.org/10.1016/j.renene.2019.10.109.
[33] Khanmohammadi S, Atashkari K, Kouhikamali R. Modeling and Assessment of a Biomass Gasification Integrated System for Multigeneration Purpose. Int J Chem Eng 2016;2016:1–11. https://doi.org/10.1155/2016/2639241.
[34] Zhang X, Zeng R, Deng Q, Gu X, Liu H, He Y, et al. Energy, exergy and economic analysis of biomass and geothermal energy based CCHP system integrated with compressed air energy storage (CAES). Energy Convers Manag 2019;199:111953. https://doi.org/10.1016/j.enconman.2019.111953.
[35] Alirahmi SM, Assareh E. Energy, exergy, and exergoeconomics (3E) analysis and multi-objective optimization of a multi-generation energy system for day and night time power generation - Case study: Dezful city. Int J Hydrogen Energy 2020;45(56):31555–73. https://doi.org/10.1016/j.ijhydene.2020.08.160.
[36] Saedpanah E, Fardi Asrami R, Sohani A, Sayyaadi H. Life cycle comparison of potential scenarios to achieve the foremost performance for an off-grid photovoltaic electri fi cation system. J Clean Prod 2020;242:118440. https://doi.org/10.1016/j.jclepro.2019.118440.
[37] Razmi AR, Arabkoohsar A, Nami H. Thermoeconomic analysis and multi-objective optimization of a novel hybrid absorption/recompression refrigeration system. Energy 2020;210:118559. https://doi.org/10.1016/j.energy.2020.118559.
[38] Bashiri Mousavi S, Adib M, Soltani M, Razmi AR, Nathwani J. Transient thermodynamic modeling and economic analysis of an adiabatic compressed air energy storage (A-CAES) based on cascade packed bed thermal energy storage with encapsulated phase change materials. Energy Convers. Manag. 2021;243:114379. https://doi.org/10.1016/j.enconman.2021.114379.
[39] Mojaver P, Khalilarya S, Chitsaz A. Multi-objective optimization and decision analysis of a system based on biomass fueled SOFC using couple method of entropy/VIKOR. Energy Convers Manag 2020;203:112260. https://doi.org/10.1016/j.enconman.2019.112260.
[40] Dincer I, Rosen MA, Ahmadi P, editors. Optimization of Energy Systems. Chichester, UK: John Wiley & Sons, Ltd; 2017.
[41] Ghorbani B, Mehrpooya M, Ardehali A. Energy and exergy analysis of wind farm integrated with compressed air energy storage using multi-stage phase change material. J Clean Prod 2020;259:120906. https://doi.org/10.1016/j.jclepro.2020.120906.
[42] Sohani A, Sayyaadi H, Zeraatpisheh M. Optimization strategy by a general approach to enhance improving potential of dew-point evaporative coolers. Elsevier 2019;188:177–213. https://doi.org/10.1016/j.enconman.2019.02.079.
[43] Alirahmi SM, Razmi AR, Arabkoohsar A. Comprehensive assessment and multi-objective optimization of a green concept based on a combination of hydrogen and compressed air energy storage (CAES) systems. Renew Sustain Energy Rev 2021;142:110850. https://doi.org/10.1016/j.rser.2021.110850.
[44] Nemati A, Nami H, Yari M, Ranjbar F, Rashid KH. Development of an exergoeconomic model for analysis and multi-objective optimization of a thermoelectric heat pump. Energy Convers Manag 2016;130:1–13. https://doi.org/10.1016/j.enconman.2016.10.045.
[45] Sanaye S, Emadi M, Refahi A. Thermal and economic modeling and optimization of a novel combined ejector refrigeration cycle. Int J Refrig 2019;98:480–93. https://doi.org/10.1016/j.ijrefrig.2018.11.007.
[46] Akrami E, Chitsaz A, Nami H, Mahmoudi SMS. Energetic and exergoeconomic assessment of a multi-generation energy system based on indirect use of geothermal energy. Energy 2017;124:625–39. https://doi.org/10.1016/j.energy.2017.02.006.
[47] Dib G, Haberschill P, Rullière R, Perroit Q, Davies S, Revellin R. Thermodynamic simulation of a micro advanced adiabatic compressed air energy storage for building application. Appl Energy 2020;260:114248. https://doi.org/10.1016/j.apenergy.2019.114248.
[48] Ebadollahi M, Rostamzadeh H, Pedram MZ, Ghaebi H, Amidpour M. Proposal and assessment of a new geothermal-based multigeneration system for cooling, heating, power, and hydrogen production, using LNG cold energy recovery. Renew Energy 2019;135:66–87. https://doi.org/10.1016/j.renene.2018.11.108.
[49] Emadi MA, Mahmoudimehr J. Modeling and thermo-economic optimization of a new multi-generation system with geothermal heat source and LNG heat sink. Energy Convers Manag 2019;189:153–66. https://doi.org/10.1016/j.enconman.2019.03.086.
[50] Nabat MH, Sharifi S, Razmi AR. Thermodynamic and economic analyses of a novel liquid air energy storage (LAES) coupled with thermoelectric generator and Kalina cycle. J Energy Storage 2022;45:103711. https://doi.org/10.1016/j.est.2021.103711.
[51] Nami H, Anvari-Moghaddam A, Arabkoohsar A, Razmi AR. 4E Analyses of a Hybrid Waste-Driven CHP–ORC Plant with Flue Gas Condensation. Sustainability 2020;12:9449. https://doi.org/10.3390/su12229449.
[52] Lazzaretto A, Toffolo A. Energy, economy and environment as objectives in multi-criterion optimization of thermal systems design. Energy 2004;29(8):1139–57. https://doi.org/10.1016/j.energy.2004.02.022.
[53] Roushenas R, Zarei E, Torabi M. A novel trigeneration system based on solid oxide fuel cell-gas turbine integrated with compressed air and thermal energy storage concepts: Energy, exergy, and life cycle approaches. Sustain Cities Soc 2021;66:102667. https://doi.org/10.1016/j.scs.2020.102667.
[54] Z. Zainal Performance and characteristics of a biomass gasifier system 1996 Cardiff University.
[55] Behzadi A, Gholamian E, Houshfar E, Habibollahzade A. Multi-objective optimization and exergoeconomic analysis of waste heat recovery from Tehran's waste-to-energy plant integrated with an ORC unit. Energy 2018;160:1055–68. https://doi.org/10.1016/j.energy.2018.07.074.